

NUMERICAL STUDY OF QUANTIZED VORTEX INTERACTIONS IN THE NONLINEAR SCHRÖDINGER EQUATION ON BOUNDED DOMAINS*

WEIZHU BAO[†] AND QINGLIN TANG[†]

Abstract. In this paper, we study numerically quantized vortex dynamics and their interactions in the two-dimensional (2D) nonlinear Schrödinger equation (NLSE) with a dimensionless parameter $\varepsilon > 0$ proportional to the size of the vortex core on bounded domains under either a Dirichlet or a homogeneous Neumann boundary condition (BC). We begin with a review of the reduced dynamical laws for time evolution of quantized vortex centers and show how to solve these nonlinear ordinary differential equations numerically. Then we outline some efficient and accurate numerical methods for discretizing the NLSE on either a rectangle or a disk under either Dirichlet or homogeneous Neumann boundary condition. Based on these efficient and accurate numerical methods for NLSE and the reduced dynamical laws, we simulate quantized vortex interactions of NLSE with different ε and different initial setups including single vortex, vortex pair, vortex dipole, and vortex cluster, compare them with those obtained from the corresponding reduced dynamical laws, and examine the validity of the reduced dynamical laws. Finally, we investigate radiation and generation of sound waves as well as their impact on vortex interactions in the NLSE dynamics.

Key words. nonlinear Schrödinger equation, quantized vortex, Dirichlet boundary condition, homogeneous Neumann boundary condition, reduced dynamical laws, time splitting

AMS subject classifications. 35Q55, 65M06, 65M70, 81Q05, 82D50

DOI. 10.1137/130906489

1. Introduction. Vortices are those waves that possess phase singularities (topological defect) and rotational flows around the singular points. They arise in many physical areas of different scales and in nature, ranging from liquid crystals and superfluids to nonequilibrium patterns and cosmic strings [14, 37]. Quantized vortices in two dimensions are those particle-like vortices whose centers are zeros of the order parameter, possessing localized phase singularity with the topological charge (also known as winding number, index, or circulation) being quantized. They have been widely observed in many different physical systems, such as liquid Helium, type-II superconductors, atomic gases, and nonlinear optics [1, 5, 13, 24, 31]. Quantized vortices are key signatures of superconductivity and superfluidity. Their study remains one of the most important and fundamental problems since they were predicted by Lars Onsager in 1947 in connection with superfluid Helium.

In this paper, we consider and study numerically quantized vortex dynamics and interactions in the two-dimensional (2D) nonlinear Schrödinger equation (NLSE), also known as the Gross–Pitaevskii equation (GPE), which is a fundamental equation for modeling and understanding superfluids [2, 16, 17, 19, 38]:

$$(1.1) \quad i\partial_t \psi^\varepsilon(\mathbf{x}, t) = \Delta \psi^\varepsilon + \frac{1}{\varepsilon^2}(1 - |\psi^\varepsilon|^2)\psi^\varepsilon, \quad \mathbf{x} \in \Omega, \quad t > 0,$$

*Received by the editors January 18, 2013; accepted for publication (in revised form) January 2, 2014; published electronically April 1, 2014. This research was supported by Singapore A*STAR SERC “Complex Systems” Research Programme grant 1224504056.

<http://www.siam.org/journals/mms/12-2/90648.html>

[†]Department of Mathematics and Center for Computational Science and Engineering, National University of Singapore, Singapore 119076, Singapore (matbaowz@nus.edu.sg, <http://www.math.nus.edu.sg/~bao/>; g0800880@nus.edu.sg).

with initial condition

$$(1.2) \quad \psi^\varepsilon(\mathbf{x}, 0) = \psi_0^\varepsilon(\mathbf{x}), \quad \mathbf{x} \in \bar{\Omega},$$

and either a Dirichlet boundary condition (BC)

$$(1.3) \quad \psi^\varepsilon(\mathbf{x}, t) = g(\mathbf{x}) = e^{i\omega(\mathbf{x})}, \quad \mathbf{x} \in \partial\Omega, \quad t \geq 0,$$

or a homogeneous Neumann BC

$$(1.4) \quad \frac{\partial \psi^\varepsilon(\mathbf{x}, t)}{\partial \mathbf{n}} = 0, \quad \mathbf{x} \in \partial\Omega, \quad t \geq 0.$$

Here, $\Omega \subset \mathbb{R}^2$ is a simply connected and bounded domain, t is time, $\mathbf{x} = (x, y) \in \mathbb{R}^2$ is the Cartesian coordinate vector, $\psi^\varepsilon := \psi^\varepsilon(\mathbf{x}, t)$ is a complex-valued function describing the “order parameter” for a superfluid, ω is a given real-valued function, ψ_0^ε and g are given smooth and complex-valued functions satisfying the compatibility condition $\psi_0^\varepsilon(\mathbf{x}) = g(\mathbf{x})$ for $\mathbf{x} \in \partial\Omega$, $\mathbf{n} = (n_1, n_2)$ and $\mathbf{n}_\perp = (-n_2, n_1) \in \mathbb{R}^2$ satisfying $|\mathbf{n}| = \sqrt{n_1^2 + n_2^2} = 1$ are the outward normal and tangent vectors along $\partial\Omega$, respectively, and $\varepsilon > 0$ is a given dimensionless constant.

Denote the Gross–Pitaevskii (GP) or Ginzburg–Landau (GL) functional (“energy”) as [11, 18, 25]

$$(1.5) \quad \mathcal{E}^\varepsilon(t) := \int_{\Omega} \left[|\nabla \psi^\varepsilon(\mathbf{x}, t)|^2 + \frac{1}{2\varepsilon^2} (|\psi^\varepsilon(\mathbf{x}, t)|^2 - 1)^2 \right] d\mathbf{x} = \mathcal{E}_{\text{kin}}^\varepsilon(t) + \mathcal{E}_{\text{int}}^\varepsilon(t);$$

then it is easy to see that, for the NLSE (1.1) with either Dirichlet BC (1.3) or homogeneous Neumann BC (1.4) for general domain Ω , or periodic BC when Ω is a rectangle, the GP functional $\mathcal{E}^\varepsilon(t)$ is conserved, i.e., $\mathcal{E}^\varepsilon(t) \equiv \mathcal{E}^\varepsilon(0)$ for $t \geq 0$.

Several analytical and numerical studies have dealt with quantized vortex states of the NLSE (1.1) and their interactions in the whole space \mathbb{R}^2 or on bounded domains under different scalings with regard to the distances between different vortices. Based on a formal analysis, Fetter [15] predicted that, to the leading order, the dynamics of vortices in the NLSE (1.1) would be governed by the same law as that in the ideal incompressible fluid. The same prediction was then given mathematically by Neu [31] using the method of matched asymptotics. In Neu’s work [31], he found vortex states of the NLSE (1.1) in the whole space \mathbb{R}^2 with $\varepsilon = 1$ for superfluidity and conjectured the stability of these states under NLSE dynamics as an open problem [31]. Based on his conjecture on the stability, he obtained formally the reduced dynamical laws governing the motion of the vortex centers under the assumption that these vortices are distinct and well-separated; i.e., the reduced dynamical laws are asymptotically valid when the distances between vortex centers become larger and larger [31]. Under this scaling, the vortex core size is $O(1)$. Based on the reduced dynamical law, which is a set of ordinary differential equations (ODEs) for the vortex centers, one can obtain that two vortices with opposite winding numbers (vortex dipole or vortex-antivortex) move in parallel, while they rotate along a circle if they have the same winding number (vortex pair). However, these ODEs are correct only up to the leading order. Corrections to this leading order approximation due to radiation and/or related questions when long-time dynamics of vortices is considered still remain an important open problem. Using the method of effective action and geometric solvability, Ovchinnikov and Sigal confirmed Neu’s approximation and derived some leading radiative corrections [34, 35] based on the assumption that the vortices are well-separated, which was

extended by Lange and Schroers [23] to the study of the dynamics of overlapping vortices. Recently, by proposing efficient and accurate numerical methods for discretizing the NLSE in the whole space, Zhang, Bao, and Du [43, 44] compared the dynamics of quantized vortices from the reduced dynamical laws obtained by Neu with those from the direct numerical simulation results of the NLSE under different parameters and/or initial setups. They solved numerically Neu's open problem on the stability of vortex states under the NLSE dynamics: vortices with winding number $m = \pm 1$ are dynamically stable and, respectively, $|m| > 1$ dynamically unstable [43, 44], which agrees with those conclusions derived asymptotically by Ovchinnikov and Sigal [33]. In addition, they identified numerically different parameter regimes that the dynamics and interactions of vortex centers obtained from the reduced dynamical laws agree qualitatively and/or quantitatively as well as fail to agree with those obtained from the NLSE dynamics [43, 44].

We remark here that Kevrekidis and his collaborators [8, 20, 28, 30, 36, 41, 42] recently carried out some very interesting works on the dynamics and structure stability of vortex clusters with several vortices in trapped Bose–Einstein condensates (BEC) by studying the GPE with confinement potentials in the whole space \mathbb{R}^2 . Due to the confinement potential and normalization condition, the situation there is different from ours: (i) the profile of each single vortex is different—the density outside the vortex core (with size at $O(\varepsilon)$) is uniform with value 1 up to the domain boundary in our case (cf. Figure 1) and it is zero outside the Thomas–Fermi radius in the BEC setup due to the harmonic confinement potential; (ii) in the strong interaction regime, i.e., $0 < \varepsilon \ll 1$, the density is almost 1 everywhere except the vortex core in our case, while it is at $O(\sqrt{\varepsilon})$ in the BEC setup when the dimensionless interaction strength in front of the cubic interaction is at $O(1/\varepsilon^2)$ [4]; (iii) there is no new vortex generated from the boundary during the dynamics due to the nonzero boundary condition in our case, while there are new vortices generated from the boundary in the BEC setup [21] due to the harmonic trapping potential. Thus the setups there are quite different from that in this paper.

Inspired by Neu's work, many researchers have published papers on the study of the vortex states and dynamics governed by the NLSE (1.1) on a bounded domain $\Omega \subset \mathbb{R}^2$ with the introduction of a small dimensionless parameter $0 < \varepsilon < 1$, which is proportional to the core size of a vortex. Under this scaling, the core size of each vortex is $O(\varepsilon)$ and the distances between vortex centers initially are $O(1)$. Mironescu [29] investigated stability of the vortices in (1.1) with (1.3) and showed that for fixed winding number m , a vortex with $|m| = 1$ is always dynamically stable, while for those of winding number $|m| > 1$, there exists a critical ε_m^c such that if $\varepsilon > \varepsilon_m^c$, the vortex is stable; otherwise it is unstable. Mironescu's results were then improved by Lin [27] using the spectrum of a linearized operator. Subsequently, Lin and Xin [25] studied the vortex dynamics on a bounded domain with either a Dirichlet or a Neumann BC, which was further investigated by Jerrard and Spirn [18] using different methods. In addition, Colliander and Jerrard [11, 12] studied the vortex structures and dynamics on a torus under a periodic BC. In these studies, the authors derived the reduced dynamical laws which govern the dynamics of vortex centers under the NLSE dynamics when $\varepsilon \rightarrow 0$ with fixed initial distances between different vortex centers. They obtained that, to the leading order, the vortices move according to the Kirchhoff law in the bounded domain case. However, these reduced dynamical laws cannot indicate radiation and/or sound propagations created by highly corotating or overlapping vortices. It remains a very fascinating and fundamental problem to understand the vortex-sound interactions [10, 32] and how the sound waves modify the motion of vortices [16].

Very recently, the authors designed some efficient and accurate numerical methods for studying vortex dynamics and interactions in the GL equation on bounded domains with either a Dirichlet or a Neumann BC [6]. These numerical methods can be extended and applied to study the rich and complicated phenomena related to vortex dynamics in the NLSE (1.1) with either Dirichlet BC (1.3) or homogeneous Neumann BC (1.4) on bounded domains. The main goals of this paper are (i) to present efficient and accurate numerical methods for discretizing the reduced dynamical laws and the NLSE (1.1) on bounded domains under different BCs, (ii) to understand numerically how the BC and radiation, as well as geometry of the domain, affect vortex dynamics and interactions, (iii) to study numerically the vortex interactions in the NLSE dynamics and/or compare them with those from the reduced dynamical laws under different initial setups and parameter regimes, and (iv) to identify cases where the vortex dynamics and interactions from the reduced dynamical laws agree/disagree qualitatively and/or quantitatively with those from the NLSE dynamics.

The rest of the paper is organized as follows. In section 2, we briefly review the reduced dynamical laws of vortex interactions under the NLSE (1.1) with either a Dirichlet or a homogeneous Neumann BC and present numerical methods to discretize them. In section 3, efficient and accurate numerical methods are briefly outlined for discretizing the NLSE on bounded domains with different BCs. In section 4, numerical results are reported for vortex interactions of the NLSE under the Dirichlet BC, and similar results for the NLSE under the homogeneous Neumann BC are reported in section 5. Finally, some conclusions are drawn in section 6.

2. The reduced dynamical laws and their discretization. In this section, we review two different forms of the reduced dynamical laws for the dynamics of vortex centers in the NLSE (1.1) with either a Dirichlet or a homogeneous Neumann BC, show their equivalence, and present efficient numerical methods to discretize them.

We assume that, in the initial data ψ_0^ε , there are exactly M isolated and distinct vortices whose centers are located at $\mathbf{x}_1^0 = (x_1^0, y_1^0)$, $\mathbf{x}_2^0 = (x_2^0, y_2^0)$, \dots , $\mathbf{x}_M^0 = (x_M^0, y_M^0)$ with winding numbers n_1, n_2, \dots, n_M , respectively. The winding number of each vortex can be chosen as either 1 or -1 , i.e., $n_j = 1$ or -1 for $j = 1, 2, \dots, M$. At time $t \geq 0$, the M isolated and distinct vortex centers are located at $\mathbf{x}_1(t) = (x_1(t), y_1(t))$, $\mathbf{x}_2(t) = (x_2(t), y_2(t))$, \dots , and $\mathbf{x}_M(t) = (x_M(t), y_M(t))$. Denote

$$X^0 := (\mathbf{x}_1^0, \mathbf{x}_2^0, \dots, \mathbf{x}_M^0), \quad X := X(t) = (\mathbf{x}_1(t), \mathbf{x}_2(t), \dots, \mathbf{x}_M(t)), \quad t \geq 0;$$

the renormalized energy associated with the M vortex centers is defined as [9, 24]

$$(2.1) \quad W(X) := W(X(t)) = - \sum_{1 \leq j \neq l \leq M} n_j n_l \ln |\mathbf{x}_j(t) - \mathbf{x}_l(t)|, \quad t \geq 0.$$

2.1. Under the Dirichlet BC. For the NLSE (1.1) with Dirichlet BC (1.3), when $\varepsilon \rightarrow 0$, two different forms of the reduced dynamical laws have been obtained in the literature for the motion of the M vortex centers.

The first, which is widely used, has been derived formally and rigorously in the literature; see, for instance, [9, 11, 22, 26] and references therein:

$$(2.2) \quad \dot{\mathbf{x}}_j(t) = -n_j J \nabla_{\mathbf{x}_j} [W(X) + W_{\text{dbc}}(X)], \quad j = 1, \dots, M, \quad t > 0,$$

with initial condition

$$(2.3) \quad \mathbf{x}_j(0) = \mathbf{x}_j^0, \quad j = 1, 2, \dots, M.$$

Here, J is a 2×2 symplectic matrix defined as

$$J = \begin{pmatrix} 0 & 1 \\ -1 & 0 \end{pmatrix},$$

and the renormalized energy $W_{\text{dbc}}(X)$ comes from the effect of the Dirichlet BC associated with the M vortex centers $X = X(t)$ and is defined as [9, 24]

$$W_{\text{dbc}}(X) = - \sum_{j=1}^M n_j R(\mathbf{x}_j; X) + \int_{\partial\Omega} \left[R(\mathbf{x}; X) + \sum_{j=1}^M n_j \ln |\mathbf{x} - \mathbf{x}_j| \right] \frac{\partial_{\mathbf{n}_\perp} \omega(\mathbf{x})}{2\pi} ds,$$

where, for any fixed $X \in \Omega^M$, $R(\mathbf{x}; X)$ is a harmonic function in \mathbf{x} , i.e.,

$$(2.4) \quad \Delta R(\mathbf{x}; X) = 0, \quad \mathbf{x} \in \Omega,$$

with the Neumann BC

$$(2.5) \quad \frac{\partial R(\mathbf{x}; X)}{\partial \mathbf{n}} = \partial_{\mathbf{n}_\perp} \omega(\mathbf{x}) - \frac{\partial}{\partial \mathbf{n}} \sum_{l=1}^M n_l \ln |\mathbf{x} - \mathbf{x}_l|, \quad \mathbf{x} \in \partial\Omega.$$

Using an identity in [9, eq. (51), p. 84],

$$\nabla_{\mathbf{x}_j} [W(X) + W_{\text{dbc}}(X)] = -2n_j \nabla_{\mathbf{x}} \left[R(\mathbf{x}; X) + \sum_{l=1 \& l \neq j}^M n_l \ln |\mathbf{x} - \mathbf{x}_l| \right]_{\mathbf{x}=\mathbf{x}_j},$$

the reduced dynamical law (2.2) can be simplified, for $1 \leq j \leq M$, to

$$(2.6) \quad \dot{\mathbf{x}}_j(t) = 2J \left[\nabla_{\mathbf{x}} R(\mathbf{x}; X) |_{\mathbf{x}=\mathbf{x}_j(t)} + \sum_{l=1 \& l \neq j}^M n_l \frac{\mathbf{x}_j(t) - \mathbf{x}_l(t)}{|\mathbf{x}_j(t) - \mathbf{x}_l(t)|^2} \right], \quad t > 0.$$

The second form of the reduced dynamical law was obtained by Lin and Xin [25] for $1 \leq j \leq M$ as

$$(2.7) \quad \dot{\mathbf{x}}_j(t) = 2J \left[J \nabla_{\mathbf{x}} H(\mathbf{x}; X) |_{\mathbf{x}=\mathbf{x}_j(t)} + \sum_{l=1 \& l \neq j}^M n_l \frac{\mathbf{x}_j(t) - \mathbf{x}_l(t)}{|\mathbf{x}_j(t) - \mathbf{x}_l(t)|^2} \right], \quad t > 0,$$

where for any fixed $X \in \Omega^M$, $H(\mathbf{x}; X)$ is a harmonic function in \mathbf{x} and satisfies the BC

$$(2.8) \quad \frac{\partial H(\mathbf{x}; X)}{\partial \mathbf{n}_\perp} = \partial_{\mathbf{n}_\perp} \omega(\mathbf{x}) - \frac{\partial}{\partial \mathbf{n}} \sum_{l=1}^M n_l \ln |\mathbf{x} - \mathbf{x}_l|, \quad \mathbf{x} \in \partial\Omega.$$

In the above two different forms of the reduced dynamical laws for the NLSE, although the two harmonic functions $R(\mathbf{x}; X)$ and $H(\mathbf{x}; X)$ satisfy different BCs, they are equivalent. In fact, they are both equivalent to the following reduced dynamical law: For $1 \leq j \leq M$,

$$(2.9) \quad \dot{\mathbf{x}}_j(t) = 2J \left[J \nabla_{\mathbf{x}} Q(\mathbf{x}; X) |_{\mathbf{x}=\mathbf{x}_j(t)} + \sum_{l=1 \& l \neq j}^M n_l \frac{\mathbf{x}_j(t) - \mathbf{x}_l(t)}{|\mathbf{x}_j(t) - \mathbf{x}_l(t)|^2} \right], \quad t > 0,$$

where, for any fixed $X \in \Omega^M$, $Q(\mathbf{x}; X)$ is a harmonic function in \mathbf{x} and satisfies the Dirichlet BC

$$(2.10) \quad Q(\mathbf{x}; X) = \omega(\mathbf{x}) - \sum_{l=1}^M n_l \theta(\mathbf{x} - \mathbf{x}_l), \quad \mathbf{x} \in \partial\Omega,$$

with the function $\theta : \mathbb{R}^2 \rightarrow [0, 2\pi)$ being defined as

$$(2.11) \quad \cos(\theta(\mathbf{x})) = \frac{x}{|\mathbf{x}|}, \quad \sin(\theta(\mathbf{x})) = \frac{y}{|\mathbf{x}|}, \quad 0 \neq \mathbf{x} = (x, y) \in \mathbb{R}^2.$$

LEMMA 2.1. *For any fixed $X \in \Omega^M$, we have the identity*

$$(2.12) \quad J\nabla_{\mathbf{x}}Q(\mathbf{x}; X) = \nabla_{\mathbf{x}}R(\mathbf{x}; X) = J\nabla_{\mathbf{x}}H(\mathbf{x}; X), \quad \mathbf{x} \in \Omega,$$

which immediately implies the equivalence of the three reduced dynamical laws (2.6), (2.7), and (2.9).

Proof. For any fixed $X \in \Omega^M$, since Q is a harmonic function, there exists a function $\varphi_1(\mathbf{x})$ such that

$$J\nabla_{\mathbf{x}}Q(\mathbf{x}; X) = \nabla\varphi_1(\mathbf{x}), \quad \mathbf{x} \in \Omega.$$

Thus, $\varphi_1(\mathbf{x})$ satisfies the Laplace equation

$$(2.13) \quad \Delta\varphi_1(\mathbf{x}) = \nabla \cdot (J\nabla_{\mathbf{x}}Q(\mathbf{x}; X)) = \partial_{yx}\varphi_1(\mathbf{x}) - \partial_{xy}\varphi_1(\mathbf{x}) = 0, \quad \mathbf{x} \in \Omega,$$

with the Neumann BC

$$(2.14) \quad \partial_{\mathbf{n}}\varphi_1(\mathbf{x}) = (J\nabla_{\mathbf{x}}Q(\mathbf{x}; X)) \cdot \mathbf{n} = \nabla_{\mathbf{x}}Q(\mathbf{x}; X) \cdot \mathbf{n}_{\perp} = \partial_{\mathbf{n}_{\perp}}Q(\mathbf{x}; X), \quad \mathbf{x} \in \partial\Omega.$$

Noting (2.10), we obtain for $\mathbf{x} \in \partial\Omega$

$$\partial_{\mathbf{n}}\varphi_1(\mathbf{x}) = \partial_{\mathbf{n}_{\perp}}\omega(\mathbf{x}) - \frac{\partial}{\partial\mathbf{n}_{\perp}} \sum_{l=1}^M n_l \theta(\mathbf{x} - \mathbf{x}_l) = \partial_{\mathbf{n}_{\perp}}\omega(\mathbf{x}) - \frac{\partial}{\partial\mathbf{n}} \sum_{l=1}^M n_l \ln|\mathbf{x} - \mathbf{x}_l|.$$

Combining the above equality with (2.13), (2.4), and (2.5), we get

$$\Delta(R(\mathbf{x}; X) - \varphi_1(\mathbf{x})) = 0, \quad \mathbf{x} \in \Omega; \quad \partial_{\mathbf{n}}(R(\mathbf{x}; X) - \varphi_1(\mathbf{x})) = 0, \quad \mathbf{x} \in \partial\Omega.$$

Thus

$$R(\mathbf{x}; X) = \varphi_1(\mathbf{x}) + \text{constant}, \quad \mathbf{x} \in \Omega,$$

which immediately implies the first equality in (2.12). The second equality in (2.12) can be proved in a similar way, but we omit it here for brevity. \square

2.2. Under the homogeneous Neumann BC. Similarly, for the NLSE (1.1) with the homogeneous Neumann BC (1.4), when $\varepsilon \rightarrow 0$, there are also two different forms of the reduced dynamical laws for the motion of the M vortex centers.

Again, by introducing the renormalized energy W_{nbc} , which comes from the effect of the homogeneous Neumann BC associated with the M vortex centers $X = X(t)$,

$$(2.15) \quad W_{\text{nbc}}(X) = - \sum_{j=1}^M n_j \tilde{R}(\mathbf{x}_j; X),$$

where, for any fixed $X \in \Omega^M$, $\tilde{R}(\mathbf{x}; X)$ is a harmonic function in \mathbf{x} and satisfies the Dirichlet BC

$$(2.16) \quad \tilde{R}(\mathbf{x}; X) = - \sum_{l=1}^M n_l \ln |\mathbf{x} - \mathbf{x}_l|, \quad \mathbf{x} \in \partial\Omega,$$

the first form has been derived formally and rigorously by several authors in the literature [11, 18, 22] as

$$(2.17) \quad \dot{\mathbf{x}}_j(t) = -n_j J \nabla_{\mathbf{x}_j} [W(X) + W_{\text{nbc}}(X)], \quad j = 1, \dots, M, \quad t > 0.$$

Using the identity

$$(2.18) \quad \nabla_{\mathbf{x}_j} [W(X) + W_{\text{nbc}}(X)] = -2n_j \nabla_{\mathbf{x}} \left[\tilde{R}(\mathbf{x}; X) + \sum_{l=1 \& l \neq j}^M n_l \ln |\mathbf{x} - \mathbf{x}_l| \right]_{\mathbf{x}_j},$$

the above reduced dynamical laws collapse for $1 \leq j \leq M$ as

$$(2.19) \quad \dot{\mathbf{x}}_j(t) = 2J \left[\nabla_{\mathbf{x}} \tilde{R}(\mathbf{x}; X) |_{\mathbf{x}=\mathbf{x}_j(t)} + \sum_{l=1 \& l \neq j}^M n_l \frac{\mathbf{x}_j(t) - \mathbf{x}_l(t)}{|\mathbf{x}_j(t) - \mathbf{x}_l(t)|^2} \right], \quad t > 0.$$

Similarly, the second form of the reduced dynamical law was obtained by Lin and Xin [25] for $1 \leq j \leq M$ as

$$(2.20) \quad \dot{\mathbf{x}}_j(t) = 2J \left[J \nabla_{\mathbf{x}} \tilde{Q}(\mathbf{x}; X) |_{\mathbf{x}=\mathbf{x}_j(t)} + \sum_{l=1 \& l \neq j}^M n_l \frac{\mathbf{x}_j(t) - \mathbf{x}_l(t)}{|\mathbf{x}_j(t) - \mathbf{x}_l(t)|^2} \right], \quad t > 0,$$

where, for any fixed $X \in \Omega^M$, $\tilde{Q}(\mathbf{x}; X)$ is a harmonic function in \mathbf{x} and satisfies the Neumann BC

$$(2.21) \quad \frac{\partial \tilde{Q}(\mathbf{x}; X)}{\partial \mathbf{n}} = - \frac{\partial}{\partial \mathbf{n}} \sum_{l=1}^M n_l \theta(\mathbf{x} - \mathbf{x}_l), \quad \mathbf{x} \in \partial\Omega.$$

Similarly to the proof of Lemma 2.1, we can establish the equivalence of the above two different forms of the reduced dynamical laws.

LEMMA 2.2. *The reduced dynamical laws (2.19) and (2.20) are equivalent.*

In order to compare the solution of the reduced dynamical laws (2.6) or (2.9) and (2.19) or (2.20) with those from the NLSE under a Dirichlet or a homogeneous Neumann BC, respectively, the ODEs (2.6) or (2.9) and (2.19) or (2.20) are discretized by the standard second order leap-frog method or fourth order Runge–Kutta method. For each fixed $X \in \Omega^M$, when the domain Ω is a rectangle, the Laplace equation (2.4) with BC (2.5) or (2.10) or (2.16) or (2.21) is discretized by the standard second order finite difference method, and, respectively, when the domain Ω is a disk, they are discretized in the θ -direction via the Fourier pseudospectral method and in the r -direction via the finite element method (FEM) with (r, θ) the polar coordinates. For details, we refer the reader to [6] but omit them here for brevity.

3. Numerical methods. In this section, we outline briefly some efficient and accurate numerical methods for discretizing the NLSE (1.1) in either a rectangle or a disk with initial condition (1.2) and either a Dirichlet or a homogeneous Neumann BC. The key ideas in our numerical methods are based on (i) applying a time-splitting method, which has been widely used for nonlinear partial differential equations (PDEs) [40] to decouple the nonlinearity in the NLSE [5, 7, 43], and (ii) adapting a proper finite difference method and/or FEM to discretize a free Schrödinger equation [5, 6].

Let $\tau := \Delta t > 0$ be the time step size, and denote $t_n = n\tau$ for $n \geq 0$. For $n = 0, 1, \dots$, from time $t = t_n$ to $t = t_{n+1}$, the NLSE (1.1) is solved in two splitting steps. One first solves

$$(3.1) \quad i\partial_t \psi^\varepsilon(\mathbf{x}, t) = \frac{1}{\varepsilon^2}(1 - |\psi^\varepsilon|^2)\psi^\varepsilon, \quad \mathbf{x} \in \Omega, \quad t \geq t_n,$$

for the time step of length τ , followed by solving

$$(3.2) \quad i\partial_t \psi^\varepsilon(\mathbf{x}, t) = \Delta \psi^\varepsilon, \quad \mathbf{x} \in \Omega, \quad t \geq t_n,$$

for the same time step. The discretization of (3.2) will be outlined later. For $t \in [t_n, t_{n+1}]$, we can easily obtain the following ODE for $\rho(\mathbf{x}, t) = |\psi^\varepsilon(\mathbf{x}, t)|^2$:

$$(3.3) \quad \partial_t \rho(\mathbf{x}, t) = 0, \quad t \geq t_n, \quad \mathbf{x} \in \Omega,$$

which implies that

$$(3.4) \quad \rho(\mathbf{x}, t) = \rho(\mathbf{x}, t_n), \quad t \geq t_n, \quad \mathbf{x} \in \Omega.$$

Plugging (3.4) into (3.1), we can integrate it exactly to get

$$(3.5) \quad \psi^\varepsilon(\mathbf{x}, t) = \psi^\varepsilon(\mathbf{x}, t_n) \exp \left[-\frac{1}{\varepsilon^2}(1 - |\psi^\varepsilon(\mathbf{x}, t_n)|^2)(t - t_n) \right], \quad t \geq t_n, \quad \mathbf{x} \in \Omega.$$

We remark here that, in practice, we always use the second order Strang splitting [40]; that is, from time $t = t_n$ to $t = t_{n+1}$, (i) evolve (3.1) for half time step $\tau/2$ with initial data given at $t = t_n$; (ii) evolve (3.2) for one step τ starting with the new data; and (iii) evolve (3.1) for half time step $\tau/2$ again with the newer data.

When $\Omega = [a, b] \times [c, d]$ is a rectangular domain, we denote $h_x = \frac{b-a}{N}$ and $h_y = \frac{d-c}{L}$, with N and L being two even positive integers as the mesh sizes in the x -direction and the y -direction, respectively. Similarly to the discretization of the gradient flow with constant coefficient [6], when the Dirichlet BC (1.3) is used for (3.2), it can be discretized by using the fourth order compact finite difference discretization for spatial derivatives followed by a Crank–Nicolson finite difference (CNFD) scheme for temporal derivatives [6], and when homogeneous Neumann BC (1.4) is used for (3.2), it can be discretized by using cosine spectral discretization for spatial derivatives followed by integrating in time *exactly* [6]. The details are omitted here for brevity. Combining the CNFD and cosine pseudospectral discretization for Dirichlet and homogeneous Neumann BCs, respectively, with the second order Strang splitting, we can obtain time-splitting Crank–Nicolson finite difference (TSCNFD) and time-splitting cosine pseudospectral (TSCP) discretizations for the NLSE (1.1) on a rectangle with Dirichlet BC (1.3) and homogeneous Neumann BC (1.4), respectively. Both TSCNFD and TSCP discretizations are unconditionally stable, second order in time, and have memory cost $O(NL)$ and computational cost $O(NL \ln(NL))$ per time step. In addition, TSCNFD is fourth order in space and TSCP is spectral order in space.

When $\Omega = \{\mathbf{x} \mid |\mathbf{x}| < R\} := B_R(\mathbf{0})$ is a disk with $R > 0$ a fixed constant, similarly to the discretization of the GPE with an angular momentum rotation [3, 5, 43] and/or the gradient flow with constant coefficient [6], it is natural to adopt the polar coordinate (r, θ) in the numerical discretization by using the standard Fourier pseudospectral method in the θ -direction [39], FEM in the r -direction, and the Crank–Nicolson method in time [3, 5, 43]. Again, the details are omitted here for brevity.

4. Numerical results under Dirichlet BC. In this section, we report numerical results for vortex interactions of the NLSE (1.1) under Dirichlet BC (1.3) and compare them with those obtained from the reduced dynamical laws (2.6) with (2.3). We study how the dimensionless parameter ε , initial setup, boundary value, and geometry of the domain Ω affect the dynamics and interactions of vortices. For a given bounded domain Ω , the NLSE (1.1) is unchanged by the rescaling $\mathbf{x} \rightarrow d\mathbf{x}$, $t \rightarrow d^2t$, and $\varepsilon \rightarrow d\varepsilon$ with d the diameter of Ω . Thus without loss of generality, hereafter, without specification, we always assume that the diameter of Ω is $O(1)$. The initial condition ψ_0^ε in (1.2) is chosen as

$$(4.1) \quad \psi_0^\varepsilon(\mathbf{x}) = \psi_0^\varepsilon(x, y) = e^{ih(\mathbf{x})} \prod_{j=1}^M \phi_{n_j}^\varepsilon(\mathbf{x} - \mathbf{x}_j^0), \quad \mathbf{x} = (x, y) \in \bar{\Omega},$$

where $M > 0$ is the total number of vortices in the initial data, $h(\mathbf{x})$ is a real-valued harmonic function corresponding to phase in-painting at $t = 0$, $\theta(\mathbf{x})$ is defined in (2.11), and for $j = 1, 2, \dots, M$, $n_j = 1$ or -1 , and $\mathbf{x}_j^0 = (x_j^0, y_j^0) \in \Omega$ are the winding number and initial location of the j th vortex, respectively. In addition,

$$\phi_{n_j}^\varepsilon(\mathbf{x}) = f^\varepsilon(|\mathbf{x}|) e^{in_j\theta(\mathbf{x})}, \quad \mathbf{x} = (x, y) \in \Omega.$$

Here, $f^\varepsilon(r)$ is chosen as

$$(4.2) \quad f^\varepsilon(r) = \begin{cases} 1, & r \geq R_0 = 0.25, \\ f_v^\varepsilon(r), & 0 \leq r \leq R_0, \end{cases}$$

where f_v^ε is the solution of the following problem:

$$\left[\frac{1}{r} \frac{d}{dr} \left(r \frac{d}{dr} \right) - \frac{1}{r^2} + \frac{1}{\varepsilon^2} (1 - (f_v^\varepsilon(r))^2) \right] f_v^\varepsilon(r) = 0, \quad 0 < r < R_0,$$

with the Dirichlet BC

$$f_v^\varepsilon(r = 0) = 0, \quad f_v^\varepsilon(r = R_0) = 1.$$

The solution f_v^ε of the above problem is computed numerically, and we depict the function $f^\varepsilon(r)$ in Figure 1 with different ε . Thus in the initial data (4.1), there are exactly M distinct vortices with core size at $O(\varepsilon)$ under a phase in-painting $h(\mathbf{x})$. The function g in the Dirichlet BC (1.3) is chosen as

$$(4.3) \quad g(\mathbf{x}) = e^{i(h(\mathbf{x}) + \sum_{j=1}^M n_j \theta(\mathbf{x} - \mathbf{x}_j^0))}, \quad \mathbf{x} \in \partial\Omega,$$

so that it is compatible with ψ_0^ε at $t = 0$.

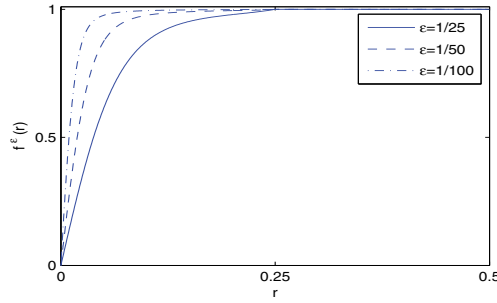


FIG. 1. Plot of the function $f^\epsilon(r)$ in (4.2) with different ϵ .

In addition, in the following sections, we mainly consider the following six different modes of the phase in-painting $h(\mathbf{x})$:

- Mode 0: $h(\mathbf{x}) = 0$.
- Mode 1: $h(\mathbf{x}) = x + y$.
- Mode 2: $h(\mathbf{x}) = x - y$.
- Mode 3: $h(\mathbf{x}) = x^2 - y^2$.
- Mode 4: $h(\mathbf{x}) = x^2 - y^2 + 2xy$.
- Mode 5: $h(\mathbf{x}) = x^2 - y^2 - 2xy$.

To simplify our presentation, for $j = 1, 2, \dots, M$, hereafter we let $\mathbf{x}_j^\epsilon(t)$ and $\mathbf{x}_j^r(t)$ be the j th vortex center in the NLSE dynamics and the corresponding reduced dynamical laws, respectively, and denote $d_j^\epsilon(t) = |\mathbf{x}_j^\epsilon(t) - \mathbf{x}_j^r(t)|$ as their difference. Furthermore, in the presentation of the figures, the initial location of a vortex with winding number $+1$, -1 and the location where two vortices merge are marked as “+”, “o”, and “ \diamond ”, respectively. Finally, in our computations, if not specified, we take $\Omega = [-1, 1]^2$ in (1.1), mesh sizes $h_x = h_y = \frac{\epsilon}{10}$, and time step $\tau = 10^{-6}$. The NLSE (1.1) with (1.3), (1.2), and (4.1) is solved by the method TSCNFD presented in section 3.

4.1. Single vortex. Here we present numerical results of the motion of a single quantized vortex in the NLSE (1.1) dynamics and the corresponding reduced dynamics; i.e., we take $M = 1$, $n_1 = 1$ in (4.1). To study how the initial phase shift $h(\mathbf{x})$ and initial location of the vortex \mathbf{x}_1^0 affect the motion of the vortex and to understand the validity of the reduced dynamical law, we consider the following 11 cases:

- Cases I–III: $\mathbf{x}_1^0 = (0, 0)$, and $h(\mathbf{x})$ is chosen as Mode 1, 2, and 3, respectively.
- Cases IV–VIII: $\mathbf{x}_1^0 = (0.1, 0)$, and $h(\mathbf{x})$ is chosen as Mode 1, 2, 3, 4, and 5, respectively.
- Cases IX–XI: $\mathbf{x}_1^0 = (0.1, 0.1)$, and $h(\mathbf{x})$ is chosen as Mode 3, 4, and 5, respectively.

Moreover, to study the effect of domain geometry, we consider Ω of three types: Type I, a square $\Omega = [-1, 1]^2$; Type II, a rectangle $\Omega = [-1, 1] \times [-0.65, 0.65]$; and Type III, a unit disk $\Omega = B_1(\mathbf{0})$. Thus we also study the following four additional cases:

- Cases XII–XIII: $\mathbf{x}_1^0 = (0, 0)$, $h(\mathbf{x}) = x + y$, and Ω is chosen as Type II and III, respectively.
- Cases XIV–XV: $\mathbf{x}_1^0 = (0.1, 0)$, $h(\mathbf{x}) = x^2 - y^2$, and Ω is chosen as Type II and III, respectively.

Figure 2 depicts the trajectory of the vortex center when $\epsilon = \frac{1}{40}$ in (1.1) for Cases I–VI and d_1^ϵ with different ϵ for Cases I, V, and VI. Figure 3 shows the trajectory of the vortex center when $\epsilon = \frac{1}{64}$ in (1.1) for Cases VI–XI, while Figure 4 shows that for Cases XII–XVII when $\epsilon = \frac{1}{32}$ in (1.1). From Figures 2–4 and additional numerical experiments (not shown here for brevity), we can draw the following conclusions:

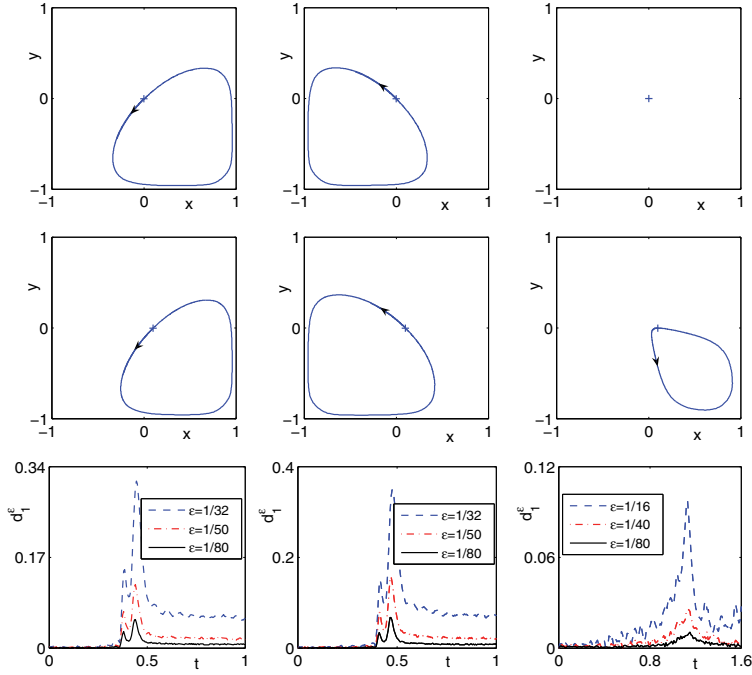


FIG. 2. Trajectory of the vortex center in NLSE under Dirichlet BC when $\varepsilon = \frac{1}{40}$ for Cases I–VI (from left to right and then from top to bottom in the top two rows), and d_1^2 for different ε for Cases I, V, and VI (from left to right in bottom row) in section 4.1.

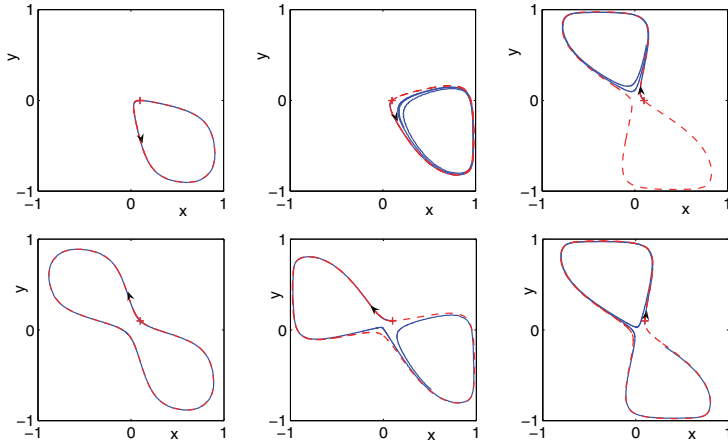


FIG. 3. Trajectory of the vortex center in NLSE dynamics under Dirichlet BC when $\varepsilon = \frac{1}{64}$ (solid line) and from the reduced dynamical laws (dashed line) for Cases VI–XI (from left to right and then from top to bottom) in section 4.1.

- (i) When $h(\mathbf{x}) \equiv 0$, the vortex center does not move, and this is similar to the case in the whole space.
- (ii) When $h(\mathbf{x}) = (x + by)(x - \frac{y}{b})$ with $b \neq 0$, the vortex does not move if $\mathbf{x}_1^0 = (0, 0)$, while it does move if $\mathbf{x}_1^0 \neq (0, 0)$ (cf. Figure 2, Cases III and VI for $b = 1$).

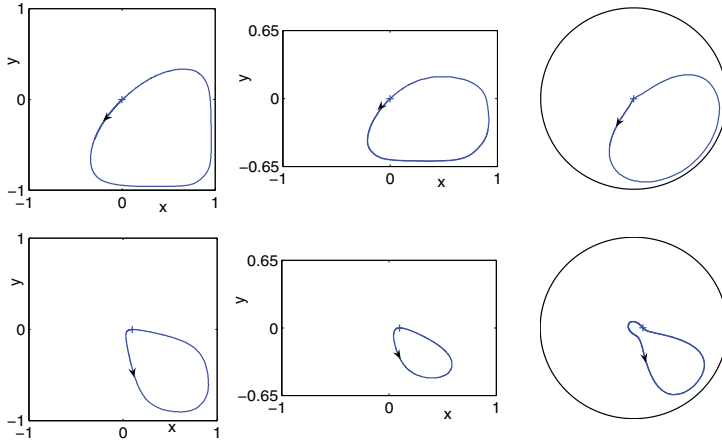


FIG. 4. Trajectory of the vortex center in the NLSE under the Dirichlet BC when $\varepsilon = \frac{1}{40}$ for Cases I, XII, XIII, VI, XIV, and XV (from left to right and then from top to bottom) in section 4.1.

(iii) When $h(\mathbf{x}) \neq 0$ and $h(\mathbf{x}) \neq (x + by)(x - \frac{y}{b})$ with $b \neq 0$, in general, the vortex center does move. For the NLSE dynamics, there exists a critical value ε_c depending on $h(\mathbf{x})$, \mathbf{x}_1^0 , and Ω such that if $\varepsilon < \varepsilon_c$, the vortex will move periodically in a closed loop (cf. Figure 2); otherwise its trajectory will not be a closed loop. This differs significantly from the situation in the reduced dynamics, where the trajectory is always periodic (cf. Figure 3, dashed line). Thus the reduced dynamical laws fail qualitatively when $\varepsilon > \varepsilon_c$. It should be an interesting problem to find out how this critical value depends on $h(\mathbf{x})$, \mathbf{x}_1^0 , and the geometry of Ω .

(iv) In general, the initial location, the geometry of the domain, and the boundary value will all affect the motion of the vortex (cf. Figure 4).

(v) When $\varepsilon \rightarrow 0$, the dynamics of the vortex center under the NLSE dynamics converges uniformly in time to that of the vortex center under the reduced dynamics (cf. Figure 2, bottom row). This verifies numerically the validation of the reduced dynamical laws.

4.2. Vortex pair. Here we present numerical results of the interactions of a vortex pair under the NLSE (1.1) dynamics and its corresponding reduced dynamical laws; i.e., we take $M = 2$, $n_1 = n_2 = 1$, $\mathbf{x}_2^0 = -\mathbf{x}_1^0 = (d_0, 0)$ with $0 < d_0 < 1$ (i.e., the two vortices are initially located symmetrically on the x -axis), $h(\mathbf{x}) \equiv 0$ in (4.1), and $\varepsilon = \frac{1}{40}$ in (1.1). Figure 5 depicts the trajectory of the vortex pair and time evolution of $\mathcal{E}^\varepsilon(t)$, $\mathcal{E}_{\text{kin}}^\varepsilon(t)$, $\mathbf{x}_1^\varepsilon(t)$, $\mathbf{x}_2^\varepsilon(t)$, and $d_1^\varepsilon(t)$ for different d_0 .

From Figure 5 and additional numerical results (not shown here for brevity), we can draw the following conclusions for the interaction of a vortex pair under NLSE dynamics (1.1) with a Dirichlet BC:

(i) The total energy is conserved numerically very well during the dynamics.

(ii) The initial locations of the two vortices affect significantly the motion of the vortex pair. If the vortex pair is symmetric initially, then they move periodically and their trajectories are symmetric, i.e., $\mathbf{x}_1^\varepsilon(t) = -\mathbf{x}_2^\varepsilon(t)$ for $t \geq 0$. Furthermore, for both the reduced dynamical law and NLSE dynamics, there exist critical values, say d_c^r and d_c^ε , respectively, such that if $d_0 < d_c^r$ (or $d_0 < d_c^\varepsilon$ in the NLSE dynamics), the two vortices will rotate with each other and move along a circle-like trajectory; otherwise,

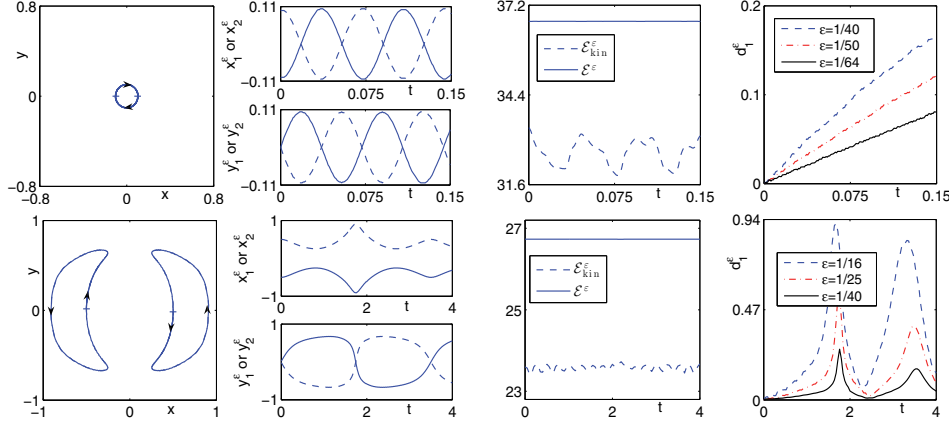


FIG. 5. Trajectory of the vortex pair (left column), time evolution of $\mathbf{x}_1^\varepsilon(t)$ and $\mathbf{x}_2^\varepsilon(t)$ (second column), $\mathcal{E}^\varepsilon(t)$ and $\mathcal{E}_{\text{kin}}^\varepsilon(t)$ (third column), and $d_1^\varepsilon(t)$ (last column) for $d_0 = 0.1$ (top row) and $d_0 = 0.5$ (bottom row) in section 4.2.

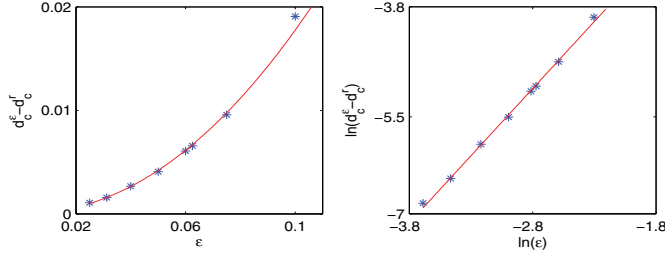


FIG. 6. Critical value d_c^ε for the interaction of a vortex pair of the NLSE (1.1) under the Dirichlet BC with $h(\mathbf{x}) = 0$ in (4.1) for different ε in section 4.2.

they will move along a crescent-like trajectory (cf. Figure 5). We find numerically the critical values $d_c^r \approx 0.4923$ and d_c^ε for $0 < \varepsilon < 1$, which are depicted in Figure 6. From these values, we obtain numerically the following relation for d_c^r and d_c^ε :

$$d_c^\varepsilon = d_c^r + 2.11\varepsilon^{2.08}, \quad 0 < \varepsilon < 1.$$

(iii) For any fixed d_0 , the dynamics of the two vortex centers under the NLSE dynamics converges uniformly in time to that of the two vortex centers under the reduced dynamical laws (cf. Figure 5) when $\varepsilon \rightarrow 0$. However, for fixed ε , the reduced dynamical law fails qualitatively to describe the motion of vortices if $d_c^r < d_0 < d_c^\varepsilon$.

4.3. Vortex dipole. Here we present numerical results of the interactions of a vortex dipole under the NLSE (1.1) dynamics and its corresponding reduced dynamical laws; i.e., we take $M = 2$, $h(\mathbf{x}) \equiv 0$, $n_1 = -n_2 = -1$, $\mathbf{x}_2^0 = -\mathbf{x}_1^0 = (d_0, 0)$ in (4.1) with $d_0 = 0.5$, and $\varepsilon = \frac{1}{25}$ in (1.1). Figure 7 depicts contour plots of $|\psi^\varepsilon(x, t)|$ at different times, trajectory of the vortex dipole, and time evolution of $\mathbf{x}_1^\varepsilon(t)$, $\mathbf{x}_2^\varepsilon(t)$, and $d_1^\varepsilon(t)$. From Figure 7 and additional numerical results (not shown here for brevity), we can draw the following conclusions:

- (i) The total energy is conserved numerically very well during the dynamics.
- (ii) The vortex dipole under the NLSE dynamics moves upward symmetrically with respect to the y -axis, and finally the two vortices in the vortex dipole merge with

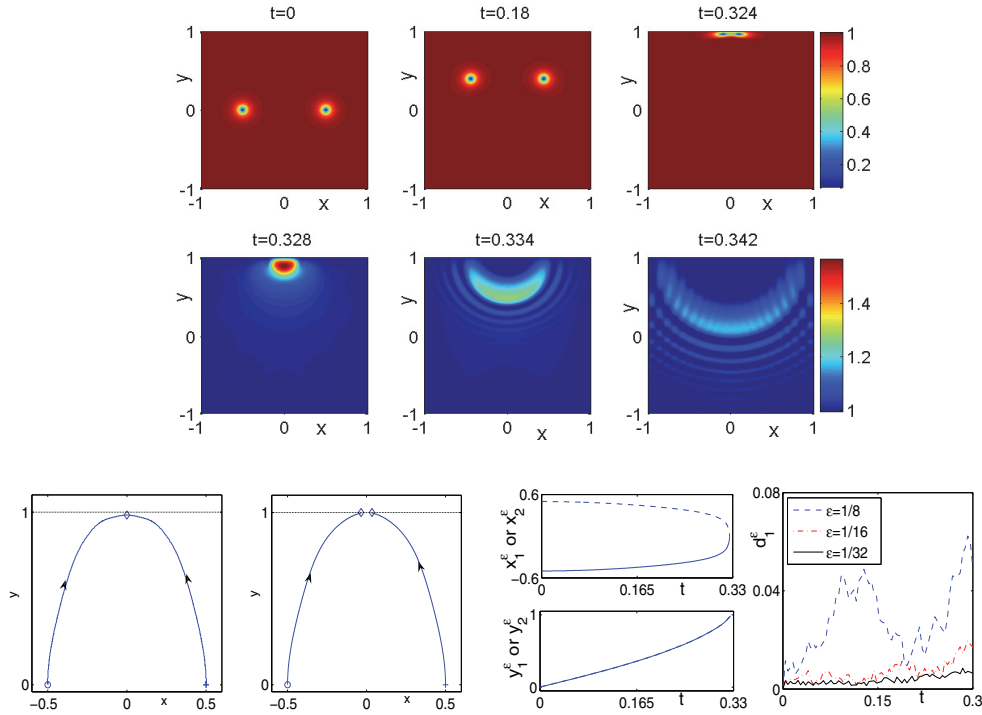


FIG. 7. Contour plots of $|\psi^\varepsilon(\mathbf{x}, t)|$ at different times (top two rows), trajectory of $\mathbf{x}_1^\varepsilon(t)$ and $\mathbf{x}_2^\varepsilon(t)$ in the NLSE dynamics (bottom left) and of $\mathbf{x}_1^r(t)$ and $\mathbf{x}_2^r(t)$ in reduced dynamics (bottom, second plot), and time evolution of $\mathbf{x}_1^\varepsilon(t)$ and $\mathbf{x}_2^\varepsilon(t)$ (bottom, third plot) and $d_1^\varepsilon(t)$ (bottom right) for the dynamics of a vortex dipole in section 4.3.

each other and they are annihilated somewhere near the top boundary simultaneously. The distance between the merging place and the boundary is $O(\varepsilon)$ when ε is small. After merging, new waves will be created and reflected by the top boundary. The new waves will then move back into the domain and be reflected back into the domain again when they hit the left, right, and bottom boundaries (cf. Figure 7). Moreover, the two vortices in the vortex dipole in the NLSE dynamics will always merge in some place near the top boundary for all d_0 (cf. Figure 7, bottom left). However, in the reduced dynamics, the two vortices never merge inside Ω (cf. Figure 7 bottom, second plot). Hence, the reduced dynamical law fails qualitatively when the vortex dipole is near the boundary.

(iii) When $\varepsilon \rightarrow 0$, the dynamics of the two vortex centers under the NLSE dynamics converges uniformly to that of the two vortex centers under the reduced dynamical laws (cf. Figure 7) before the two vortices merge with each other or are near the boundary. Again, this verifies numerically the validation of the reduced dynamical laws in this case. In fact, based on our extensive numerical experiments, the motion of the two vortex centers from the reduced dynamical laws agrees with that of the two vortices from the NLSE dynamics qualitatively when $0 < \varepsilon < 1$ and quantitatively when $0 < \varepsilon \ll 1$ when the two vortices are not too close to the boundary.

4.4. Vortex cluster. Here we present numerical studies on the dynamics of vortex clusters in the NLSE (1.1) with Dirichlet BC (1.3); i.e., we choose the initial

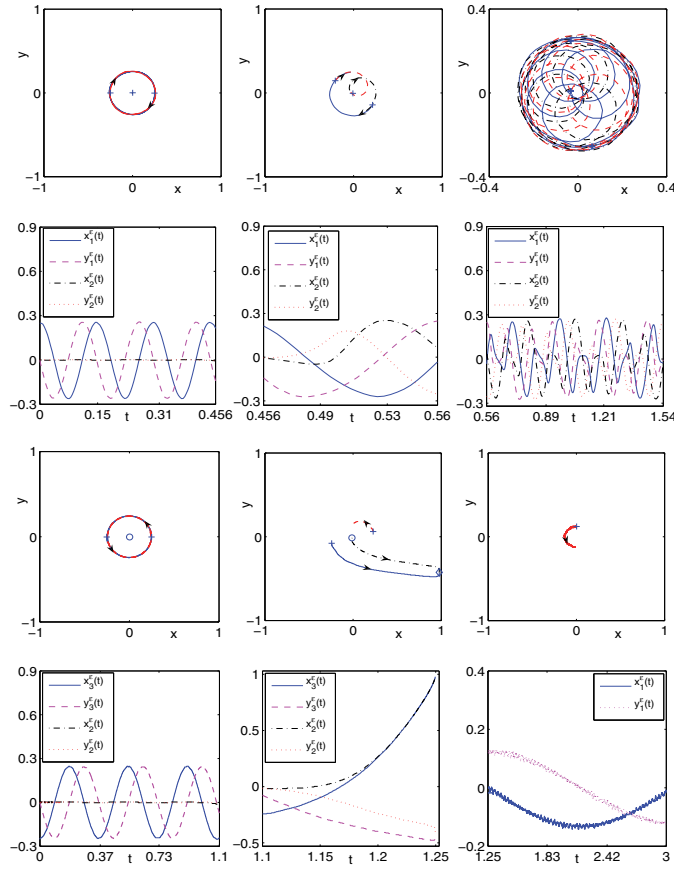


FIG. 8. Trajectory of the vortex \mathbf{x}_1^ε (solid line), \mathbf{x}_2^ε (dashed-dotted line), and \mathbf{x}_3^ε (dashed line) (first and third rows) and their corresponding time evolution (second and fourth rows) for Case I (top two rows) and Case II (bottom two rows) for small time (left column), intermediate time (middle column), and large time (right column) with $\varepsilon = \frac{1}{40}$ and $d_0 = 0.25$ in section 4.4.

data (1.2) as (4.1) and study the following four cases:

Case I. $M = 3, n_1 = n_2 = n_3 = 1, \mathbf{x}_1^0 = -\mathbf{x}_3^0 = (d_0, 0)$, and $\mathbf{x}_2^0 = (0, 0)$.

Case II. $M = 3, n_1 = -n_2 = n_3 = 1, \mathbf{x}_1^0 = -\mathbf{x}_3^0 = (d_0, 0)$, and $\mathbf{x}_2^0 = (0, 0)$.

Case III. $M = 4, n_1 = n_2 = -n_3 = -n_4 = 1, \mathbf{x}_1^0 = -\mathbf{x}_2^0 = (d_1, 0)$, and $\mathbf{x}_3^0 = -\mathbf{x}_4^0 = (0, d_2)$ with $0 < d_1, d_2 < 1$.

Case IV. $\Omega = B_5(\mathbf{0}), M = 9, n_1 = n_2 = \dots = n_9 = 1$, and the nine vortex centers are initially located on the 3×3 uniform mesh points for the rectangle $[-d_0, d_0]^2$ with $0 < d_0 < 1$.

Figure 8 depicts the trajectory and time evolution of $\mathbf{x}_1^\varepsilon(t), \mathbf{x}_2^\varepsilon(t)$, and $\mathbf{x}_3^\varepsilon(t)$ in the NLSE dynamics for Cases I and II. Figure 9 shows contour plots of $|\psi^\varepsilon|$ at different times in the NLSE dynamics for Case III, and Figure 10 depicts contour plots of $-|\psi^\varepsilon|$, as well as slice plots of $|\psi^\varepsilon(x, 0, t)|$, showing sound wave propagation of the NLSE dynamics in Case IV. Based on Figures 8–10 and additional computations (not shown here for brevity), we can draw the following conclusions:

(i) For Case I, the middle vortex (initially at the origin) will not move, while the other two vortices rotate clockwise around the origin for some time. This dynamics

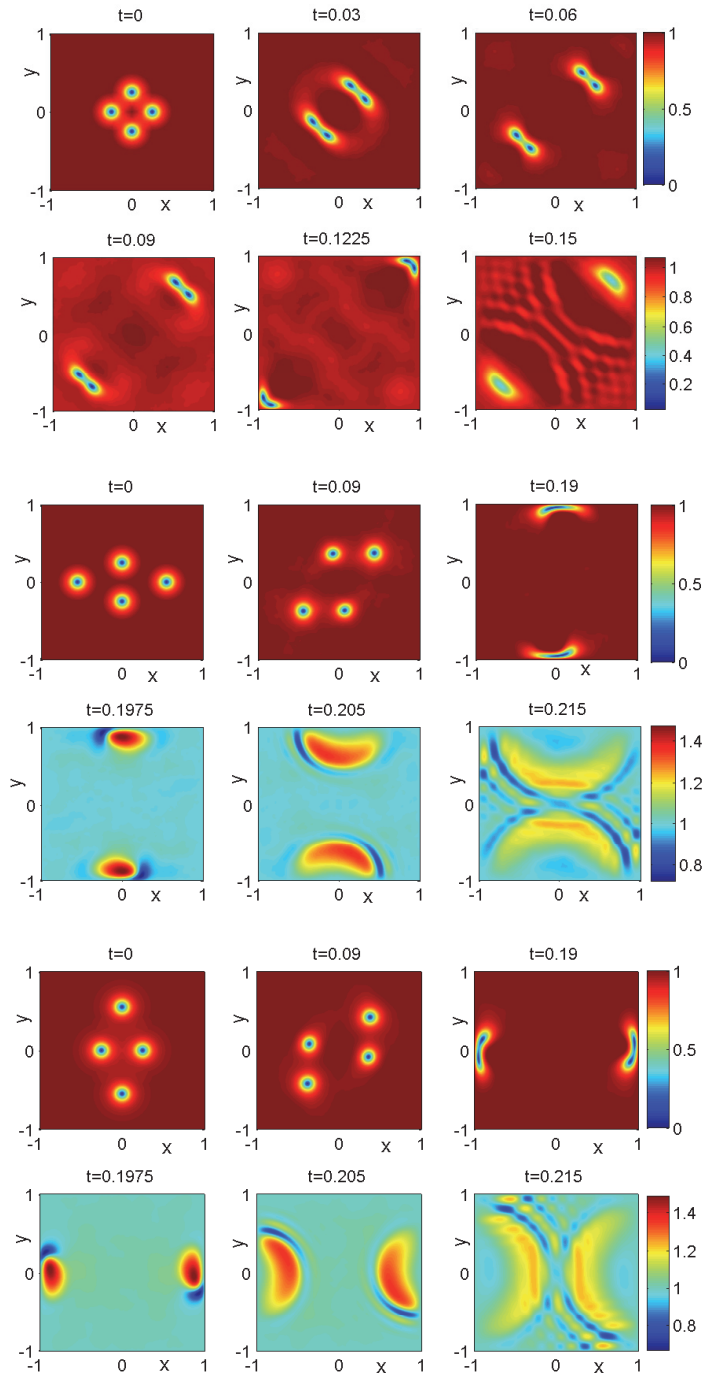


FIG. 9. Contour plots of $|\psi^\varepsilon(\mathbf{x}, t)|$ with $\varepsilon = \frac{1}{16}$ at different times for the NLSE dynamics of a vortex cluster in Case III with different initial locations: $d_1 = d_2 = 0.25$ (top two rows); $d_1 = 0.55$, $d_2 = 0.25$ (middle two rows); $d_1 = 0.25$, $d_2 = 0.55$ (bottom two rows) in section 4.4.

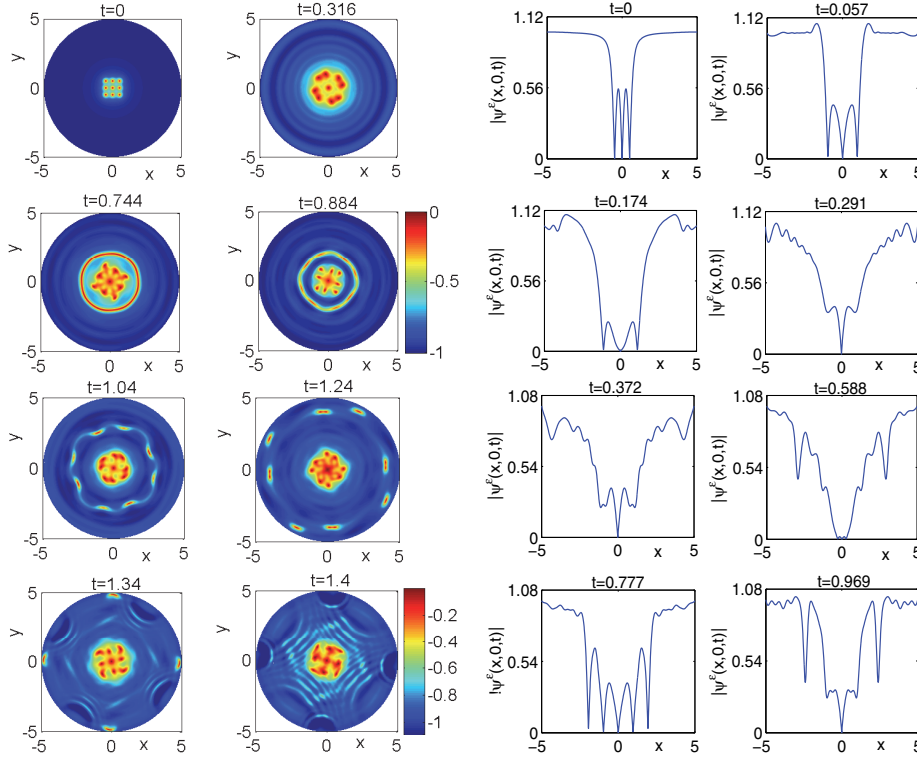


FIG. 10. Contour plots of $-\psi^\epsilon(\mathbf{x}, t)$ (left) and slice plots of $|\psi^\epsilon(x, 0, t)|$ (right) at different times showing sound wave propagation under the NLSE dynamics of a vortex cluster in Case IV with $d_0 = 0.5$ and $\epsilon = \frac{1}{8}$ in section 4.4.

agrees very well with the NLSE dynamics in the whole plane [43, 44]. After some time, the above symmetric structure is broken due to boundary effect and numerical errors; i.e., the middle vortex will begin to move toward one of the other two vortices and form a pair of vortices, then the two vortices in the pair will rotate with each other and the vortex pair will rotate with the leftover single vortex for a while. Then this pair will separate and one of them will form a new vortex pair with the single vortex, while the other becomes a new single vortex rotating with them. This process will be repeated tautologically like three dancers exchanging their partners alternatively. The dynamical pattern after the symmetric structure breaking depends highly on the mesh size and time step chosen.

(ii) For Case II, similarly to Case I, the middle vortex (initially at the origin) will not move, while the other two vortices rotate counterclockwise around the origin for some time. This dynamics agrees very well with the NLSE dynamics in the whole plane [43, 44]. After some time, again the above symmetric structure is broken due to boundary effect and numerical errors; i.e., the middle vortex will begin to move toward one of the other two vortices and form a vortex dipole which will move nearly parallel to the boundary and merge near the boundary. Sound waves will be created and reflected back into the domain and will drive the leftover vortex in the domain to move (cf. Figure 8). Again the dynamical pattern after the symmetric structure breaking depends highly on the mesh size and time step chosen. From section 4.1, we

know that a single vortex in the NLSE with $h(\mathbf{x}) = 0$ does not move, and hence this example illustrates clearly the vortex-sound interactions which cannot be predicted by the reduced dynamical laws since they are valid only before annihilation and when ε is very small.

(iii) For Case III, the four vortices form two vortex dipoles when t is small. Then the two dipoles move outward in opposite directions, and finally the two vortices in each vortex dipole merge and are annihilated at some place near the boundary. If $d_1 = d_2$, the two vortex dipoles move symmetrically with respect to the line $y = x$ and the two vortices in each dipole merge some place near the top-right and bottom-left corners, respectively; if $d_1 > d_2$, they move to the top boundary and the bottom boundary, respectively, and again the two vortices in each dipole merge with each other when they are close to the boundary; and if $d_1 < d_2$, they move to the left boundary and the right boundary, respectively, and again the two vortices in each dipole merge with each other when they are close to the boundary. New waves are created after the two vortices in each dipole merge with each other and are reflected back into the domain when they hit the boundary (cf. Figure 9).

(iv) For Case IV, vortex (initially at the origin) does not move due to symmetry, while the other eight vortices rotate clockwise and move along two circular trajectories (cf. Figure 10). During the dynamics, sound waves are generated and they propagate outward, and are reflected back into the domain when they hit the boundary. The distances between the one centered at the origin and the other eight vortices increase when sound waves are radiated outward; on the other hand, they decrease and become even smaller than their initial distances when sound waves are reflected by the boundary and move back into the domain (cf. Figure 10). This example clearly shows the impact of sound waves on the dynamics of vortices.

Similarly to the case in BEC setups [20, 28, 36, 42], the symmetric structure near $t = 0$ in Cases I and II for three vortices is dynamically unstable; i.e., symmetric structure breaking will happen very quickly if we perturb the location of either the central vortex or one of the side vortices a little bit. To show this, we perturb the initial locations of some vortices in Case I to the following:

Type I. Asymmetric perturbation: \mathbf{x}_2^0 from $(0, 0) \rightarrow (\delta, 0)$ with $\delta > 0$.

Type II. Asymmetric perturbation: \mathbf{x}_1^0 from $(d_0, 0) \rightarrow (d_0 - \delta, 0)$ with $\delta > 0$.

Type III. Symmetric perturbation: \mathbf{x}_1^0 from $(d_0, 0) \rightarrow (d_0 - \delta, 0)$ and \mathbf{x}_3^0 from $(-d_0, 0) \rightarrow (-d_0 + \delta, 0)$ with $\delta > 0$.

Figure 11 depicts the trajectory of $\mathbf{x}_1^\varepsilon(t)$, $\mathbf{x}_2^\varepsilon(t)$, and $\mathbf{x}_3^\varepsilon(t)$ as well as $d_2^\varepsilon(t) := |\mathbf{x}_2^\varepsilon(t)|$ for the above three perturbations. From this figure and additional computations (not shown here for brevity), we see that the symmetric structure is dynamically stable under a symmetric perturbation, and it is dynamically unstable under a small asymmetric perturbation. For more stability analysis of vortex clusters, we refer the reader to [8, 20, 28, 30, 36, 41, 42] and references therein.

4.5. Radiation and sound wave. Here we study numerically how the radiation and sound waves affect the dynamics of quantized vortices in the NLSE dynamics under the Dirichlet BC. To this end, we consider two types of perturbation.

Type I: Perturbation on the initial data; i.e., we take the initial data (1.2) as

$$(4.4) \quad \psi^\varepsilon(\mathbf{x}, 0) = \psi_0^{\delta, \varepsilon}(\mathbf{x}) = \psi_0^\varepsilon(\mathbf{x}) + \delta e^{-10((|x|-0.08)^2 + y^2)}, \quad \mathbf{x} = (x, y) \in \Omega,$$

where ψ_0^ε is given as in (4.1) with $h(\mathbf{x}) \equiv 0$, $M = 2$, $n_1 = n_2 = 1$, and $\mathbf{x}_1^0 = -\mathbf{x}_2^0 = (0, 1, 0)$; i.e., we perturb the initial data for studying the interactions of a vortex pair by a Gaussian function with amplitude δ . Then we take $\delta = \varepsilon$ and let ε go to 0 and

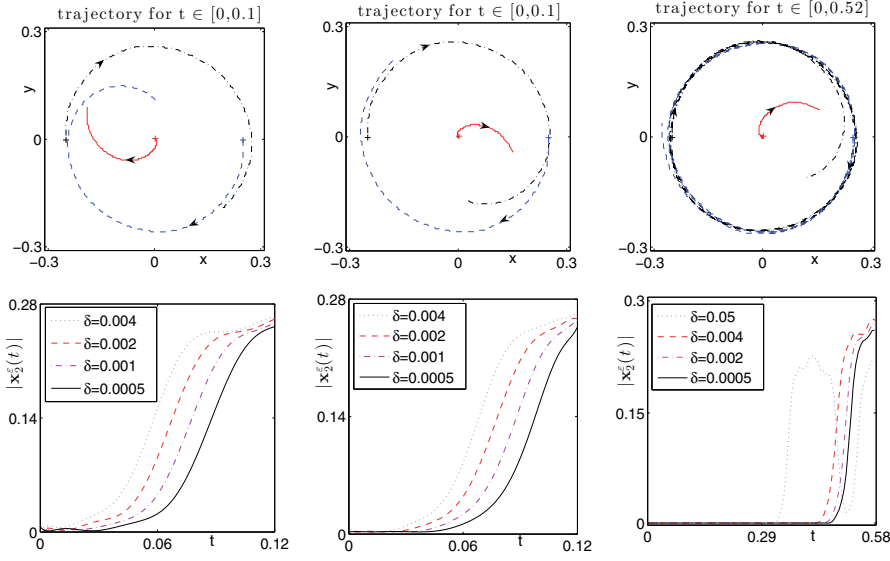


FIG. 11. Trajectory of the vortex centers $\mathbf{x}_1^\varepsilon(t)$ (dashed line), $\mathbf{x}_2^\varepsilon(t)$ (solid line), and $\mathbf{x}_3^\varepsilon(t)$ (dashed-dotted line) with $\delta = 0.0005$ (top row) and time evolution of the distance of \mathbf{x}_2^ε to the origin, i.e., $|\mathbf{x}_2^\varepsilon(t)|$ for different δ (bottom row) under the NLSE dynamics with $\varepsilon = \frac{1}{40}$ and $d_0 = 0.25$ for perturbation Type I (first column), Type II (second column), and Type III (third column) in section 4.4.

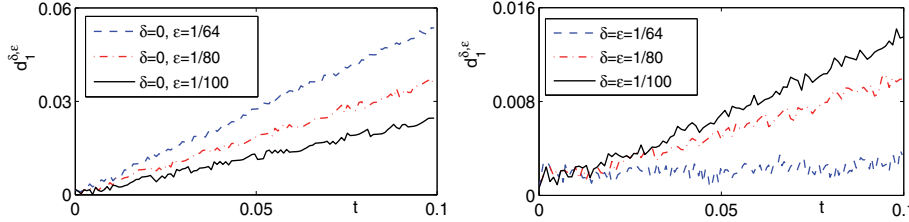


FIG. 12. Time evolution of $d_1^{\delta, \varepsilon}(t)$ for nonperturbed initial data (left) and perturbed initial data (right) in section 4.5.

solve the NLSE (1.1) with initial condition (4.4) for the vortex centers $\mathbf{x}_1^{\delta, \varepsilon}(t)$ and $\mathbf{x}_2^{\delta, \varepsilon}(t)$ and compare them with those from the reduced dynamical law. We denote $d_j^{\delta, \varepsilon}(t) = |x_j^{\delta, \varepsilon}(t) - x_j^r(t)|$ for $j = 1, 2$ as the error. Figure 12 depicts time evolution of $d_1^{\delta, \varepsilon}(t)$ for the case when $\delta = \varepsilon$, i.e., small perturbation, and the case when $\delta = 0$, i.e., no perturbation. From this figure, we can see that the dynamics of the two vortex centers under the NLSE dynamics converges to that of the two vortex centers obtained from the reduced dynamical law when $\varepsilon \rightarrow 0$ without perturbation (cf. Figure 12, left). On the contrary, the two vortex centers under the NLSE dynamics do not converge to those obtained from the reduced dynamical law when $\varepsilon \rightarrow 0$ with small perturbation (cf. Figure 12, right). This clearly demonstrates radiation and sound wave effects on vortices in the NLSE dynamics with the Dirichlet BC.

Type II: Perturbation by an external potential; i.e., we replace the uniform

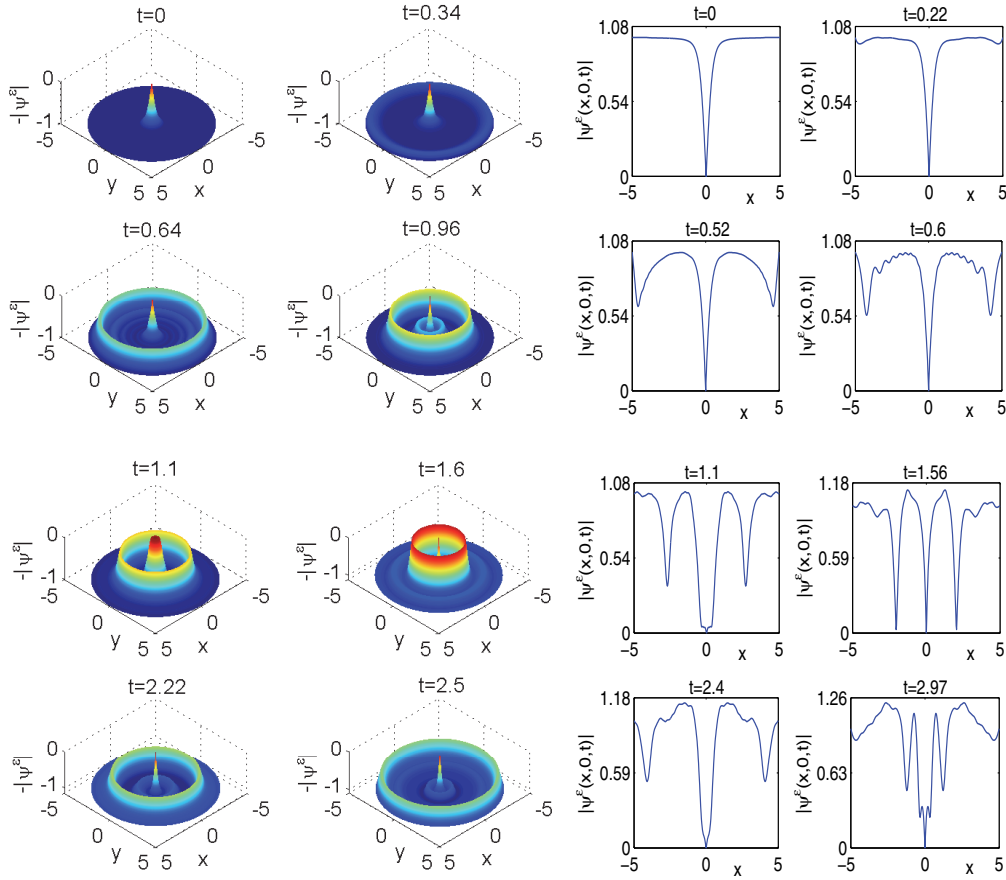


FIG. 13. Surface plots of $-\lvert\psi^\epsilon(\mathbf{x}, t)\rvert$ (left) and slice plots of $\lvert\psi^\epsilon(x, 0, t)\rvert$ (right) at different times showing sound wave propagation under the NLSE dynamics in a disk with $\epsilon = \frac{1}{4}$ and a perturbation in the potential in section 4.5.

potential in (1.1) by a nonuniform potential and solve the NLSE

$$(4.5) \quad i\partial_t \psi^\epsilon(\mathbf{x}, t) = \Delta \psi^\epsilon + \frac{1}{\epsilon^2}(1 - W(\mathbf{x}, t) - |\psi^\epsilon|^2)\psi^\epsilon, \quad \mathbf{x} \in \Omega, \quad t > 0,$$

with

$$(4.6) \quad W(\mathbf{x}, t) = \begin{cases} -\sin(2t)^2, & t \in [0, 0.5], \\ 0, & t > 0.5, \end{cases} \quad \mathbf{x} \in \Omega.$$

The initial data is chosen as (4.1) with $M = 1$, $n_1 = 1$, $\mathbf{x}_1^0 = (0, 0)$, $\Omega = B_5(\mathbf{0})$, and $\epsilon = \frac{1}{4}$. In fact, the perturbation is introduced when $t \in [0, 0.5]$ and is removed after $t = 0.5$. Figure 13 illustrates surface plots of $-\lvert\psi^\epsilon\rvert$ and slice plots of $\psi^\epsilon(x, 0, t)$ at different times showing sound wave propagation. From Figure 13, we can see that the perturbed vortex configuration rotates and radiates sound waves. This agrees well with some former prediction in the whole plane, for example, in Lange and Schroers [23] for the case $M = 2$. The waves will be reflected back into the domain when they hit the boundary and then be absorbed by the vortex core. Then the

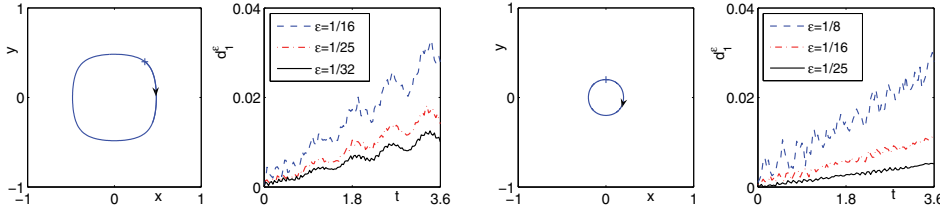


FIG. 14. Trajectory of the vortex center when $\varepsilon = \frac{1}{32}$ and time evolution of d_1^ε for different ε for the motion of a single vortex in NLSE under the homogeneous Neumann BC with $\mathbf{x}_1^0 = (0.35, 0.4)$ (left two figures) or $\mathbf{x}_1^0 = (0, 0.2)$ (right two figures) in (5.1) in section 5.1.

vortex core will radiate new waves and the process is repeated tautologically. This process explicitly illustrates the radiation in the NLSE dynamics.

Remark 4.1. Based on this example and other numerical results (not shown here for brevity), we can conclude that the vortex with winding number $m = \pm 1$ is dynamically stable under the NLSE dynamics in a bounded domain with a perturbation in the initial data and/or external potential. Meanwhile, we also found numerically that the vortex with winding number $m = 2$ and $\varepsilon = \frac{1}{32}$ is also dynamically stable under a perturbation in the external potential. Actually, Mironescu [29] indicated that for a vortex with winding number $|m| > 1$, there exists a critical value ε_m^c such that if $\varepsilon < \varepsilon_m^c$, the vortex is unstable; otherwise the vortex is stable. It was also numerically observed that a vortex with $|m| > 1$ is unstable under a perturbation in the potential but stable under a perturbation in the initial data in the whole plane case [43]. Hence, it would be an interesting problem to investigate numerically how the stability of a vortex depends on its winding number, value of ε , and strength and/or type of the perturbation under the NLSE dynamics on bounded domains.

5. Numerical results under Neumann BC. In this section, we report numerical results for vortex interactions of the NLSE (1.1) under the homogeneous Neumann BC (1.4) and compare them with those obtained from the reduced dynamical laws (2.19) with (2.3). The initial condition ψ_0^ε in (1.2) is chosen as

$$(5.1) \quad \psi_0^\varepsilon(\mathbf{x}) = \psi_0^\varepsilon(x, y) = e^{ih_n(\mathbf{x})} \prod_{j=1}^M \phi_{n_j}^\varepsilon(\mathbf{x} - \mathbf{x}_j^0), \quad \mathbf{x} = (x, y) \in \bar{\Omega},$$

where $h_n(\mathbf{x})$ is a harmonic function satisfying the Neumann BC

$$\frac{\partial}{\partial \mathbf{n}} h_n(\mathbf{x}) = -\frac{\partial}{\partial \mathbf{n}} \sum_{l=1}^M n_l \theta(\mathbf{x} - \mathbf{x}_l^0), \quad \mathbf{x} \in \partial\Omega.$$

In fact, the choice of $h_n(\mathbf{x})$ is such that ψ_0^ε satisfies the homogeneous Neumann BC (1.4). The NLSE (1.1) with (1.4), (1.2), and (5.1) is solved by the TSCP method presented in section 3.

5.1. Single vortex. Here we present numerical results of the motion of a single quantized vortex under the NLSE (1.1) dynamics and its corresponding reduced dynamical laws, i.e., we take $M = 1$ and $n_1 = 1$ in (5.1). Figure 14 depicts trajectory of the vortex center for different \mathbf{x}_1^0 in (5.1) when $\varepsilon = \frac{1}{32}$ in (1.1) and d_1^ε for different ε . From Figure 14 and additional numerical results (not shown here for brevity), we can see the following:

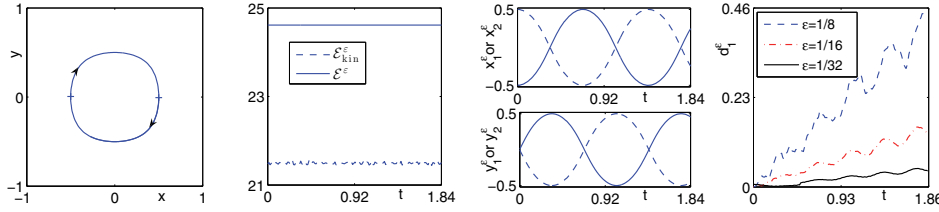


FIG. 15. Trajectory of the vortex pair (left), time evolution of \mathcal{E}^ε and $\mathcal{E}_{\text{kin}}^\varepsilon$ (second figure), $\mathbf{x}_1^\varepsilon(t)$ and $\mathbf{x}_2^\varepsilon(t)$ (third figure), and $d_1^\varepsilon(t)$ (right) in the NLSE dynamics under homogeneous Neumann BC with $\varepsilon = \frac{1}{32}$ and $d_0 = 0.5$ in section 5.2.

(i) If $\mathbf{x}_1^0 = (0, 0)$, the vortex will not move for all times; otherwise, the vortex will move, and its initial location \mathbf{x}_1^0 does not affect its motion qualitatively. Actually, it moves periodically in a circle-like trajectory centered at the origin when $|\mathbf{x}_1^0|$ is small, and, respectively, a square-like trajectory when $|\mathbf{x}_1^0| = O(1)$, which clearly shows the effect of the boundary. This is quite different from the situation in bounded domains with the Dirichlet BC where the motion of a single vortex depends significantly on its initial location for some $h(\mathbf{x})$. It is also quite different from the situation in the whole space where a single vortex does not move at all under the initial condition (5.1) when $\Omega = \mathbb{R}^2$.

(ii) As $\varepsilon \rightarrow 0$, the dynamics of the vortex center under the NLSE dynamics converges uniformly in time to that of the vortex center under the reduced dynamical laws. In fact, based on our extensive numerical experiments, the motion of the vortex center from the reduced dynamical laws agrees with that of the vortex centers from the NLSE dynamics qualitatively when $0 < \varepsilon < 1$ and quantitatively when $0 < \varepsilon \ll 1$.

5.2. Vortex pair. Here we present numerical results of the interactions of a vortex pair under the NLSE (1.1) dynamics and its corresponding reduced dynamical laws; i.e., we take $M = 2$, $n_1 = n_2 = 1$, and $\mathbf{x}_2^0 = -\mathbf{x}_1^0 = (d_0, 0)$ with $0 < d_0 < 1$ in (5.1). Figure 15 depicts the trajectory of the vortex pair, time evolution of $\mathcal{E}^\varepsilon(t)$, $\mathcal{E}_{\text{kin}}^\varepsilon(t)$, $\mathbf{x}_1^\varepsilon(t)$, $\mathbf{x}_2^\varepsilon(t)$, and $d_1^\varepsilon(t)$ when $\varepsilon = \frac{1}{32}$ in (1.1) and $d_0 = 0.5$ in (5.1).

From Figure 15 and additional numerical results (not shown here for brevity), we can draw the following conclusions for the interactions of a vortex pair under the NLSE dynamics (1.1) with the homogeneous Neumann BC:

(i) The total energy is conserved numerically very well during the dynamics.

(ii) The two vortices in the vortex pair move periodically along a circle-like trajectory centered at the origin when d_0 is small, and, respectively, a square-like trajectory when $d_0 = O(1)$, which clearly show the effect of the boundary. In addition, the trajectories are symmetric.

(iii) When $\varepsilon \rightarrow 0$, the dynamics of the two vortex centers under the NLSE dynamics converges uniformly in time to that of two vortex centers under the reduced dynamical laws. This verifies numerically the validation of the reduced dynamical laws in this case. In fact, based on our extensive numerical experiments, the motion of the two vortex centers from the reduced dynamical laws agrees with that of the two vortex centers from the NLSE dynamics qualitatively when $0 < \varepsilon < 1$ and quantitatively when $0 < \varepsilon \ll 1$.

5.3. Vortex dipole. Here we present numerical results of the interactions of a vortex dipole under the NLSE (1.1) dynamics and its corresponding reduced dynamical laws; i.e., we take $M = 2$, $n_1 = -n_2 = -1$, $\mathbf{x}_2^0 = -\mathbf{x}_1^0 = (d_0, 0)$ with different d_0 ,

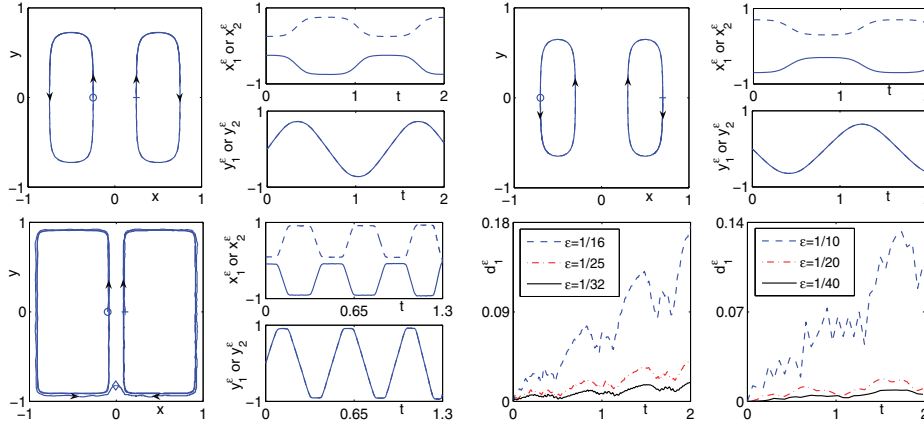


FIG. 16. Trajectory and time evolution of $\mathbf{x}_1^\epsilon(t)$ and $\mathbf{x}_2^\epsilon(t)$ for $d_0 = 0.25$ (top left two figures), $d_0 = 0.7$ (top right two figures), and $d_0 = 0.1$ (bottom left two figures), and time evolution of $d_1^\epsilon(t)$ for $d_0 = 0.25$ and $d_0 = 0.7$ (bottom right two figures) in section 5.3.

and $\varepsilon = \frac{1}{32}$ in (1.1). Figure 16 depicts the trajectory of the vortex dipole, and time evolution of $\mathbf{x}_1^\epsilon(t)$, $\mathbf{x}_2^\epsilon(t)$, and $d_1^\epsilon(t)$.

From Figure 16 and additional numerical results (not shown here for brevity), we can draw the following conclusions for the interactions of a vortex dipole under the NLSE dynamics (1.1) with the homogeneous Neumann BC:

- (i) The total energy is conserved numerically very well during the dynamics.
- (ii) The pattern of the motion of the two vortices depends on their initial locations.
- (iii) The two vortices will move symmetrically (and periodically if they are well separated) with respect to the y -axis. Moreover, there exists a critical value $d_c^r = d_c^\varepsilon = d_c$ for $0 < \varepsilon < 1$, which is found numerically as $d_c = 0.5$, such that if initially $d_0 < d_c$,

the two vortices will move first upward toward the top boundary, then turn outward to the side boundary, and finally move counterclockwise and clockwise, respectively (cf. Figure 16). While if $d_0 > d_c$, then they will move first downward toward the bottom boundary, then turn inward to the domain, and finally move counterclockwise and clockwise, respectively (cf. Figure 16). Certainly, when $d_0 = 0.5$, the vortex dipole does not move due to symmetry.

(iv) For fixed $0 < \varepsilon < 1$, there exists another critical value \hat{d}_c^ε satisfying $\lim_{\varepsilon \rightarrow 0} \hat{d}_c^\varepsilon = 0$ such that if $d_0 < \hat{d}_c^\varepsilon$, the two vortices in the dipole under the NLSE dynamics will merge at a finite time T_c depending on ε and d_0 (cf. Figure 16). However, the two vortices in the dipole from the reduced dynamical laws never merge at finite time. Hence, the reduced dynamical laws fail qualitatively if $0 < d_0 < \hat{d}_0^\varepsilon$.

(v) For fixed d_0 , when $\varepsilon \rightarrow 0$, the dynamics of the two vortex centers in the NLSE dynamics converges uniformly in time to that of the two vortex centers in the reduced dynamical laws before the two vortices merge with each other (cf. Figure 16), which verifies numerically the validation of the reduced dynamical laws in this case. In fact, based on our extensive numerical experiments, the motion of the two vortex centers from the reduced dynamical laws agrees with that of the two vortex centers in the NLSE dynamics qualitatively when $0 < \varepsilon < 1$ and quantitatively when $0 < \varepsilon \ll 1$.

5.4. Vortex cluster. Here we present numerical studies on the dynamics of vortex clusters in the NLSE (1.1) with homogeneous Neumann BC; i.e., we choose

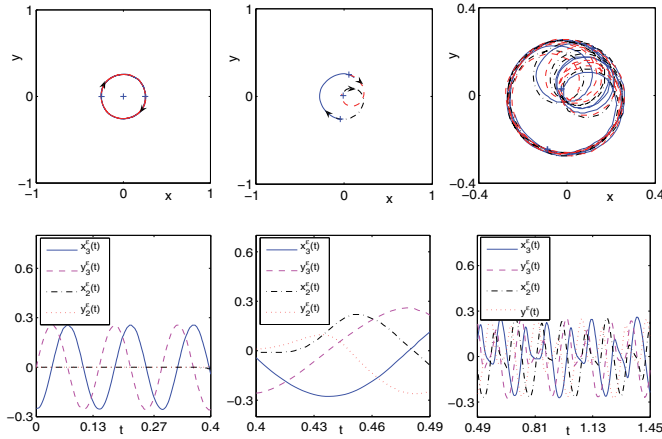


FIG. 17. Trajectory of the vortex \mathbf{x}_1^ε (solid line), \mathbf{x}_2^ε (dashed-dotted line), and \mathbf{x}_3^ε (dashed line) and their corresponding time evolution for Case I during small time (left column), intermediate time (middle column), and large time (right column) with $\varepsilon = \frac{1}{40}$ and $d_0 = 0.25$ in section 5.4.

the initial data (1.2) as (5.1) and study the following four cases:

Case I. $M = 3, n_1 = n_2 = n_3 = 1, \mathbf{x}_1^0 = -\mathbf{x}_3^0 = (d_0, 0),$ and $\mathbf{x}_2^0 = (0, 0).$

Case II. $M = 4, n_1 = n_2 = n_3 = n_4 = 1, \mathbf{x}_1^0 = -\mathbf{x}_2^0 = (d_1, 0),$ and $\mathbf{x}_3^0 = -\mathbf{x}_4^0 = (d_2, 0)$ with $0 < d_1 \neq d_2 < 1.$

Case III. $M = 4, n_1 = n_2 = -n_3 = -n_4 = 1, \mathbf{x}_1^0 = -\mathbf{x}_2^0 = (d_1, 0),$ and $\mathbf{x}_3^0 = -\mathbf{x}_4^0 = (0, d_2)$ with $0 < d_1, d_2 < 1.$

Case IV. $M = 9, n_1 = \dots = n_9 = 1,$ and the vortex centers are initially located on the 3×3 uniform mesh points for the rectangle $[-d_0, d_0]^2$ with $0 < d_0 < 1.$

Figure 17 shows trajectory and time evolution of $\mathbf{x}_1^\varepsilon(t), \mathbf{x}_2^\varepsilon(t),$ and $\mathbf{x}_3^\varepsilon(t)$ in the NLSE dynamics for Case I. Figure 18 depicts contour plots of $|\psi^\varepsilon|$ at different times in NLSE dynamics for Cases II and III, and Figure 19 shows contour plots of $-|\psi^\varepsilon|$ and slice plots of $|\psi(0, y, t)|$ in NLSE dynamics for Case IV showing sound wave propagation. Based on Figures 17–19 and additional results (not shown here for brevity), we can draw the following conclusions:

(i) For Case I, the dynamics of the vortices is quite similar to that of the vortices under the Dirichlet BC in section 4.4 and that of the vortices in the trapped BEC [8, 30, 41]. The middle vortex (initially at the origin) will not move, while the other two vortices rotate clockwise around the origin for some time. This dynamics agrees very well with the NLSE dynamics in the whole plane [43, 44]. After some time, the above symmetric structure is broken due to boundary effect and numerical errors; i.e., the middle vortex will begin to move toward one of the other two vortices and form a pair of vortices, then the two vortices in the pair will rotate with each other and the vortex pair will rotate with the leftover single vortex for a while. Then this pair will separate and one of them will form a new vortex pair with the single vortex, leaving the other to be a new single vortex rotating with the new vortex pair. This process will be repeated tautologically like three dancers exchanging their partners alternatively. In fact, the dynamical pattern after the symmetric structure breaking depends highly on the mesh size and time step.

(ii) For Case II, the four vortices form as two vortex pairs when t is small. These two pairs rotate with each other clockwise; meanwhile, the two vortices in each pair

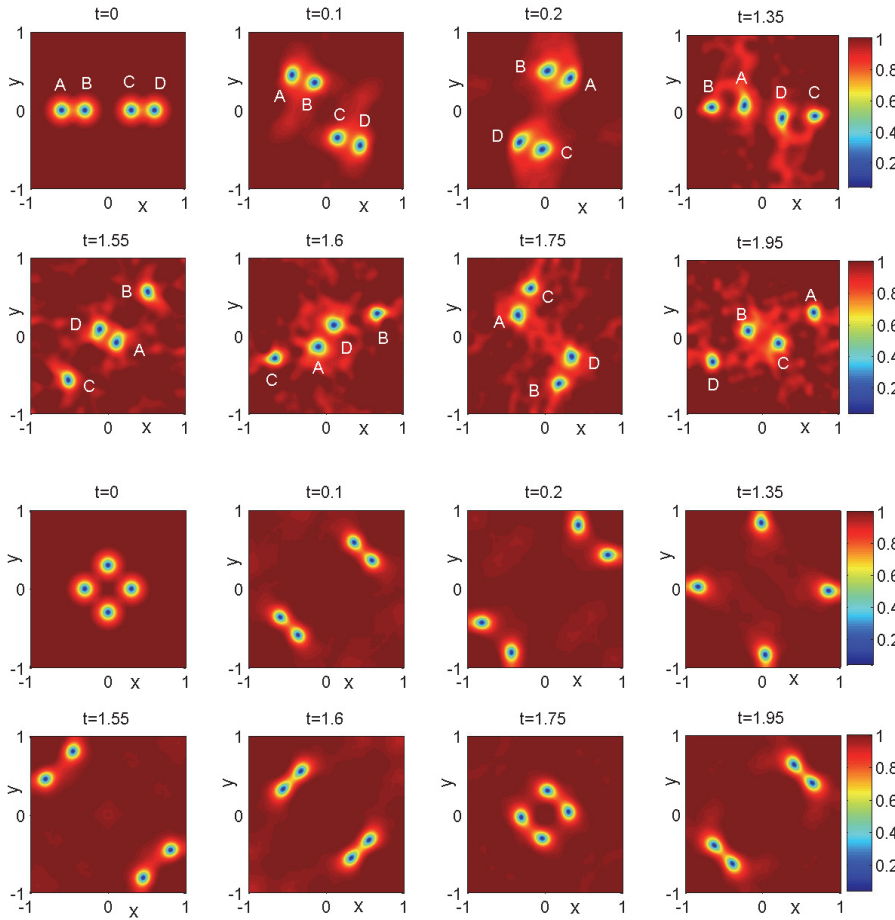


FIG. 18. Contour plots of $|\psi^\varepsilon(\mathbf{x}, t)|$ with $\varepsilon = \frac{1}{16}$ at different times for the NLSE dynamics of a vortex cluster for Case II with $d_1 = 0.6, d_2 = 0.3$ (top two rows) and Case III with $d_1 = d_2 = 0.3$ (bottom two rows) in section 5.4.

also rotate with each other clockwise, and radiations and sound waves are emitted. The sound waves propagate outward and are reflected back into the domain when they hit the boundary, which push the two vortex pairs closer. When the two vortex pairs get close enough, the two vortices with the smallest distance among the four form a new vortex pair and leave the remaining two as single vortices. The vortex pair rotates around the origin. This process is iteratively repeated during the dynamics (cf. Figure 18, top two rows).

(iii) For Case III, when t is small, the four vortices form two vortex dipoles and move symmetrically with respect to the line $y = -x$ toward the top right and bottom left corners, respectively. Meanwhile, the two vortices in each dipole move symmetrically with respect to the line $y = x$. After a while, and when the two dipoles arrive at some place near the corners, the two vortices in each dipole split from each other and reformulate two different dipoles. After this, the two vortices in each dipole move symmetrically with respect to the line $y = -x$, and the two new dipoles then

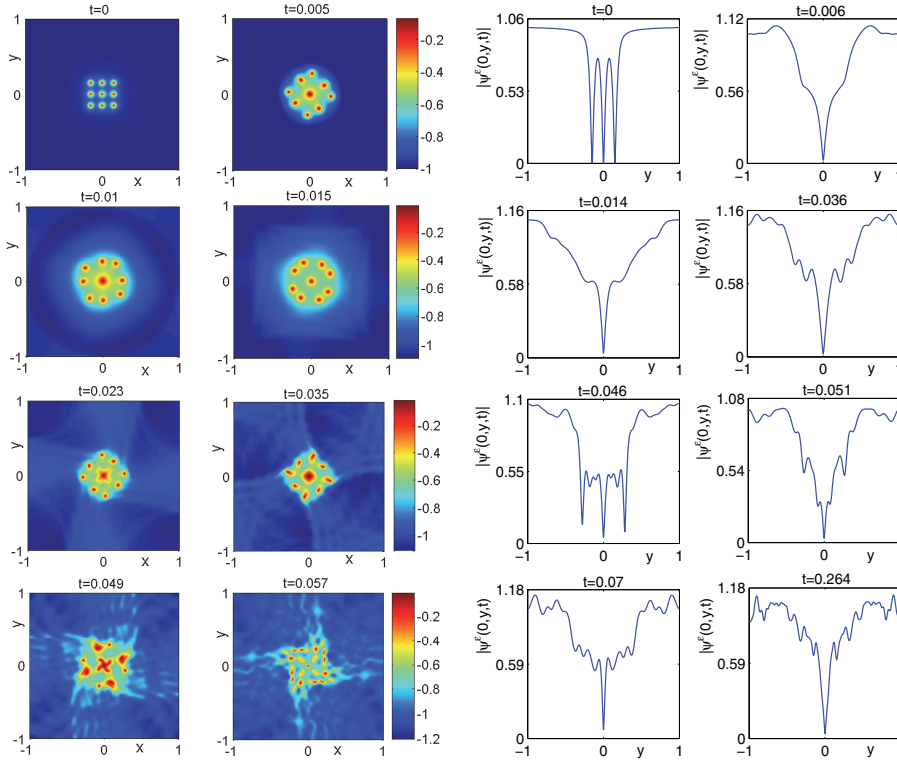


FIG. 19. Contour plots of $-\psi^\epsilon(\mathbf{x}, t)$ (left) and slice plots of $|\psi^\epsilon(0, y, t)|$ (right) at different times under the NLSE dynamics of a vortex cluster in Case IV with $d_0 = 0.15$ and $\epsilon = \frac{1}{40}$ showing sound wave propagation in section 5.4.

move symmetrically with respect to the line $y = x$ toward their initial locations. This process is then repeated periodically (cf. Figure 18, bottom two rows).

(iv) For Case IV, the vortex initially centered at the origin does not move due to symmetry, and the other eight vortices rotate clockwise and move along two circle-like trajectories (cf. Figure 19). During the dynamics, sound waves are generated and propagate outward. Some of the sound waves will exit out of the domain, while others are reflected back into the domain when they hit the boundary. The distances between the one located at the origin and the other eight vortices become larger when the sound waves are radiated outward, while they decrease when the sound waves are reflected from the boundary and move back into the domain (cf. Figure 19).

Again, similarly to the case in BEC setups [20, 28, 36, 42], the symmetric structure near $t = 0$ in Case I for three vortices is dynamically unstable, i.e., symmetric structure breaking will happen very quickly if we perturb the location of either the central vortex or one of the side vortices a little bit.

5.5. Radiation and sound wave. Here we study numerically how the radiation and sound waves affect the dynamics of quantized vortices in the NLSE dynamics under the homogeneous Neumann BC. To this end, we take the initial data (1.2) as (4.4) with ψ_0^ϵ chosen as (5.1) with $M = 2$, $n_1 = n_2 = 1$, and $\mathbf{x}_1^0 = -\mathbf{x}_2^0 = (0.1, 0)$; i.e., we perturb the initial data for studying the interactions of a vortex pair by a Gaussian function with amplitude δ . Then we take $\delta = \epsilon$, let ϵ go to 0, and solve

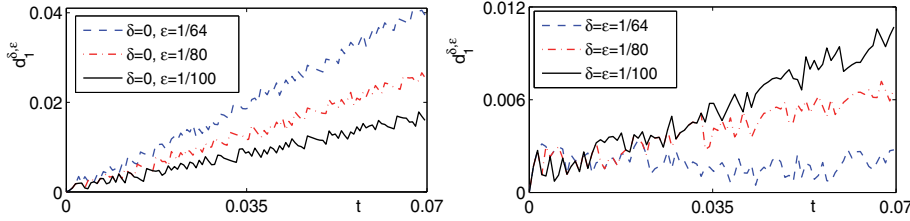


FIG. 20. Time evolution of $d_1^{\delta, \epsilon}(t)$ for nonperturbed initial data (left) and perturbed initial data (right) in section 5.5.

the NLSE (1.1) with the initial condition (4.4) for the vortex centers $\mathbf{x}_1^{\delta, \epsilon}(t)$ and $\mathbf{x}_2^{\delta, \epsilon}(t)$, and compare them with those from the reduced dynamical law. We denote $d_j^{\delta, \epsilon}(t) = |x_j^{\delta, \epsilon}(t) - x_j^r(t)|$ for $j = 1, 2$ as the error. Figure 20 depicts time evolution of $d_1^{\delta, \epsilon}(t)$ for the case when $\delta = \epsilon$, i.e., small perturbation, and the case when $\delta = 0$, i.e., no perturbation. From this figure, we can see that the dynamics of the two vortex centers under the NLSE dynamics converges to that of the two vortex centers obtained from the reduced dynamical law when $\epsilon \rightarrow 0$ without perturbation (cf. Figure 20, left). On the contrary, the two vortex centers under the NLSE dynamics do not converge to those obtained from the reduced dynamical law when $\epsilon \rightarrow 0$ with small perturbation (cf. Figure 20, right). This clearly demonstrates the radiation and sound wave effect on vortices under the NLSE dynamics with the homogeneous Neumann BC.

6. Conclusion. We studied numerically quantized vortex dynamics and their interactions in the nonlinear Schrödinger equation (NLSE) or the Gross–Pitaevskii equation (GPE) with a dimensionless parameter $0 < \epsilon < 1$ on bounded domains under either a Dirichlet or a homogeneous Neumann BC for superfluidity. Based on our extensive numerical results, we have (i) verified that the dynamics of vortex centers under the NLSE dynamics converges that of the vortex centers in the reduced dynamical laws when $\epsilon \rightarrow 0$ before the vortices collide and/or move too close to the boundary; (ii) identified parameter regimes that the motion of vortices in the reduced dynamical laws agree/disagree quantitatively and/or qualitatively with from that of vortices in the NLSE dynamics; and (iii) observed clearly radiation and sound wave effects on quantized vortex interactions under the NLSE dynamics on bounded domains.

Acknowledgments. Part of this work was done when the first author was visiting Beijing Computational Science Research Center in 2012, and he acknowledges Professor Fang-Hua Lin for the stimulating discussion. We thank the anonymous referees for their fruitful comments and suggestions on improving the paper.

REFERENCES

[1] B. P. ANDERSON, *Experiment with vortices in superfluid atomic gases*, J. Low Temp. Phys., 161 (2010), pp. 574–602.
 [2] I. S. ARANSON AND L. KRAMER, *The world of the complex Ginzburg–Landau equation*, Rev. Mod. Phys., 74 (2002), pp. 99–133.
 [3] W. BAO, *Numerical methods for the nonlinear Schrödinger equation with nonzero far-field conditions*, Methods Appl. Anal., 11 (2004), pp. 367–388.
 [4] W. BAO AND Y. CAI, *Mathematical theory and numerical methods for Bose-Einstein condensation*, Kinet. Relat. Models, 6 (2013), pp. 1–135.

- [5] W. BAO, Q. DU, AND Y. ZHANG, *Dynamics of rotating Bose–Einstein condensates and its efficient and accurate numerical computation*, SIAM J. Appl. Math., 66 (2006), pp. 758–786.
- [6] W. BAO AND Q. TANG, *Numerical study of quantized vortex interaction in the Ginzburg–Landau equation on bounded domains*, Commun. Comput. Phys., 14 (2013), pp. 819–850.
- [7] W. BAO, S. JIN, AND P. A. MARKOWICH, *On time-splitting spectral approximations for the Schrödinger equation in the semiclassical regime*, J. Comput. Phys., 175 (2002), pp. 487–524.
- [8] A. M. BARRY AND P. G. KEVREKIDIS, *Few-Particle Vortex Cluster Equilibria in Bose-Einstein Condensates: Existence and Stability*, preprint, arXiv:1306.1545v2, 2013.
- [9] F. BETHUEL, H. BREZIS, AND F. HÉLEIN, *Ginzburg–Landau Vortices*, Birkhäuser Boston, Inc., Boston, MA, 1994.
- [10] F. BETHUEL, G. ORLANDI, AND D. SMETS, *Collisions and phase-vortex interactions in dissipative Ginzburg–Landau dynamics*, Duke Math. J., 130 (2005), pp. 523–614.
- [11] J. E. COLLIANDER AND R. L. JERRARD, *Ginzburg–Landau vortices: Weak stability and Schrödinger equation dynamics*, J. Anal. Math., 77 (1999), pp. 129–205.
- [12] J. E. COLLIANDER AND R. L. JERRARD, *Vortex dynamics for the Ginzburg–Landau–Schrödinger equation*, Internat. Math. Res. Notices, 1998, no. 7, pp. 333–358.
- [13] R. J. DONNELLY, *Quantized Vortices in Helium II*, Cambridge University Press, Cambridge, UK, 1991.
- [14] A. S. DESYATNIKOV, Y. S. KIVSHAR, AND L. TORNER, *Optical vortices and vortex solitons*, Prog. Optics, 47 (2005), pp. 291–391.
- [15] A. L. FETTER, *Vortices in an imperfect Bose gas. IV. Translational velocity*, Phys. Rev., 151 (1966), pp. 100–104.
- [16] T. FRISCH, Y. POMEAU, AND S. RICA, *Transition to dissipation in a model of superflow*, Phys. Rev. Lett., 69 (1992), pp. 1644–1647.
- [17] V. GINZBURG AND L. PITAEVSKII, *On the theory of superfluidity*, Soviet Physics JETP, 34 (1958), pp. 858–861.
- [18] R. L. JERRARD AND D. SPIRN, *Refined Jacobian estimates and the Gross-Pitaevskii equations*, Arch. Ration. Mech. Anal., 190 (2008), pp. 425–475.
- [19] C. JOSSER AND Y. POMEAU, *Generation of vortices in a model superfluid He^4 by the KP instability*, Europhys. Lett., 30 (1995), pp. 43–48.
- [20] P. G. KEVREKIDIS, R. CARRETERO-GONZÁLEZ, D. J. FRANTZESKAKIS, AND I. G. KEVREKIDIS, *Vortices in Bose–Einstein condensates: Some recent developments*, Mod. Phys. Lett. B, 18 (2004), pp. 1481–1505.
- [21] A. KLEIN, D. JAKSCH, Y. ZHANG, AND W. BAO, *Dynamics of vortices in weakly interacting Bose–Einstein condensates*, Phys. Rev. A, 76 (2007), 043602.
- [22] M. KURZKE, C. MELCHER, R. MOSER, AND D. SPIRN, *Dynamics for Ginzburg–Landau vortices under a mixed flow*, Indiana Univ. Math. J., 58 (2009), pp. 2597–2622.
- [23] O. LANGE AND B. J. SCHROERS, *Unstable manifolds and Schrödinger dynamics of Ginzburg–Landau vortices*, Nonlinearity, 15 (2002), pp. 1471–1488.
- [24] F. H. LIN, *Some dynamical properties of Ginzburg–Landau vortices*, Comm. Pure Appl. Math., 49 (1996), pp. 323–359.
- [25] F. H. LIN AND J. X. XIN, *On the incompressible fluid limit and the vortex motion law of the nonlinear Schrödinger equation*, Comm. Math. Phys., 200 (1999), pp. 249–274.
- [26] F. H. LIN AND J. X. XIN, *A unified approach to vortex motion laws of complex scalar field equations*, Math. Res. Lett., 5 (1998), pp. 455–460.
- [27] T. C. LIN, *The stability of the radial solution to the Ginzburg–Landau equation*, Comm. PDE, 22 (1997), pp. 619–632.
- [28] S. MIDDELKAMP, P. G. KEVREKIDIS, D. J. FRANTZESKAKIS, R. CARRETERO-GONZÁLEZ, AND P. SCHMELCHER, *Bifurcations, stability and dynamics of multiple matter-wave vortex states*, Phys. Rev. A, 82 (2010), 013646.
- [29] P. MIRONESCU, *On the stability of radial solutions of the Ginzburg–Landau equation*, J. Funct. Anal., 130 (1995), pp. 334–344.
- [30] R. NAVARRO, R. CARRETERO-GONZÁLEZ, P. J. TORRES, P. G. KEVREKIDIS, D. J. FRANTZESKAKIS, M. W. RAY, E. ALTUNTAS, AND D. S. HALL, *Dynamics of a few co-rotating vortices in Bose–Einstein condensates*, Phys. Rev. Lett., 110 (2013), 225301.
- [31] J. NEU, *Vortices in complex scalar fields*, Phys. D, 43 (1990), pp. 385–406.
- [32] C. NORE, M. E. BRACHET, E. CERDA, AND E. TIRAPEGUI, *Scattering of first sound by superfluid vortices*, Phys. Rev. Lett., 72 (1994), pp. 2593–2595.
- [33] Y. N. OVCHINNIKOV AND I. M. SIGAL, *Ginzburg–Landau equation I. Static vortices*, in Partial Differential Equations and Their Applications, CRM Proc. Lecture Notes 12, Amer. Math. Soc., Providence, RI, 1997, pp. 199–220.

- [34] Y. N. OVCHINNIKOV AND I. M. SIGAL, *The Ginzburg-Landau equation III. Vortex dynamics*, *Nonlinearity*, 11 (1998), pp. 1277–1294.
- [35] Y. N. OVCHINNIKOV AND I. M. SIGAL, *Long-time behaviour of Ginzburg-Landau vortices*, *Nonlinearity*, 11 (1998), pp. 1295–1309.
- [36] D. E. PELINOVSKY AND P. G. KEVREKIDIS, *Variational approximations of trapped vortices in the large density limit*, *Nonlinearity*, 14 (2011), pp. 1271–1289.
- [37] L. M. PISMEN, *Vortices in Nonlinear Fields*, Clarendon, Oxford, UK, 1999.
- [38] L. PITAEVSKII, *Vortex lines in an imperfect Bose gas*, *Soviet Physics JETP*, 13 (1961), pp. 451–454.
- [39] J. SHEN AND T. TANG, *Spectral and High-Order Method with Applications*, Science Press Beijing, Beijing, 2006.
- [40] G. STRANG, *On the construction and comparison of difference schemes*, *SIAM J. Numer. Anal.*, 5 (1968), pp. 506–517.
- [41] P. J. TORRES, R. CARRETERO-GONZÁLEZ, S. MIDDELKAMO, P. SCHMELCHER, D. J. FRANTZESKAKIS, AND P. G. KEVREKIDIS, *Vortex interaction dynamics in trapped Bose-Einstein condensates*, *Comm. Pure Appl. Anal.*, 10 (2011), pp. 1589–1615.
- [42] P. J. TORRES, P. G. KEVREKIDIS, D. J. FRANTZESKAKIS, R. CARRETERO-GONZÁLEZ, P. SCHMELCHER, AND D. S. HALL, *Dynamics of vortex dipoles in confined Bose-Einstein condensates*, *Phys. Lett. A*, 375 (2011), pp. 3044–3050.
- [43] Y. ZHANG, W. BAO, AND Q. DU, *Numerical simulation of vortex dynamics in Ginzburg-Landau-Schrödinger equation*, *European J. Appl. Math.*, 18 (2007), pp. 607–630.
- [44] Y. ZHANG, W. BAO, AND Q. DU, *The dynamics and interaction of quantized vortices in the Ginzburg-Landau-Schrödinger equation*, *SIAM J. Appl. Math.*, 67 (2007), pp. 1740–1775.